Int J Earth Sci (Geol Rundsch) (2018) 107:203–229
https://doi.org/10.1007/s00531-017-1485-6

ORIGINAL PAPER

# Permian high-temperature metamorphism in the Western Alps (NW Italy)

**Barbara E. Kunz[1] · Paola Manzotti[1,2] · Brigitte von Niederhäusern[1] · Martin Engi[1] · James R. Darling[1,3] · Francesco Giuntoli[1,4] · Pierre Lanari[1]**

Received: 10 October 2016 / Accepted: 23 April 2017 / Published online: 24 May 2017


**Abstract** During the late Palaeozoic, lithospheric thinning in part of the Alpine realm caused high-temperature low-to-medium pressure metamorphism and partial melting in the lower crust. Permian metamorphism and magmatism has extensively been recorded and dated in the Central, Eastern, and Southern Alps. However, Permian metamorphic ages in the Western Alps so far are constrained by very few and sparsely distributed data. The present study fills this gap. We present U/Pb ages of metamorphic zircon from several Adria-derived continental units now situated in the Western Alps, defining a range between 286 and 266 Ma. Trace element thermometry yields temperatures of 580–890 °C from Ti-in-zircon and 630–850 °C from Zr-in-rutile for Permian metamorphic rims. These temperature estimates, together with preserved mineral assemblages (garnet–prismatic sillimanite–biotite–plagioclase–quartz–K-feldspar–rutile), define pervasive upper-amphibolite to granulite facies conditions for Permian metamorphism. U/Pb ages from this study are similar to Permian ages reported for the Ivrea Zone in the Southern Alps and Austroalpine units in the Central and Eastern Alps. Regional comparison across the former Adriatic and European margin reveals a complex pattern of ages reported from late Palaeozoic magmatic and metamorphic rocks (and relics thereof): two late Variscan age groups (~330 and ~300 Ma) are followed seamlessly by a broad range of Permian ages (300–250 Ma). The former are associated with late-orogenic collapse; in samples from this study these are weakly represented. Clearly, dominant is the Permian group, which is related to crustal thinning, hinting to a possible initiation of continental rifting along a passive margin.

**Keywords** Permian HT metamorphism · Western Alps · Adriatic margin · Zircon geochronology

## Introduction

Polymetamorphic basement rocks are exposed along the entire Alpine chain (e.g., Schmid et al. 2004; von Raumer et al. 2013). Variscan and Permian metamorphic and magmatic rocks are abundant (e.g., Marotta and Spalla 2007; von Raumer et al. 2013; Spalla et al. 2014), though only as relics where Alpine metamorphic overprint is strong. Following the Variscan orogeny, the Alpine realm underwent extension and lithospheric thinning, associated with regional high-temperature (HT) medium/low-pressure metamorphism in the lower and mid continental crust, as well as widespread magmatism at all crustal levels. Evidence of metamorphism associated with Permo-Triassic lithospheric thinning is widely documented in the Eastern and Central Alps (e.g., Schuster and Frank 1999; Thöni 1999; Schuster et al. 2001a; Hermann and Rubatto 2003; Gaidies et al. 2008a; Schuster and Stüwe 2008; Thöni and Miller 2009; Galli et al. 2011, 2012; Petri 2014). In

**Electronic supplementary material** The online version of this article (doi:10.1007/s00531-017-1485-6) contains supplementary material, which is available to authorized users.

✉ Barbara E. Kunz
barbara.kunz@geo.unibe.ch

[1] Institute of Geological Sciences, University of Bern, Baltzerstrasse 1 + 3, 3012 Bern, Switzerland

[2] Institute of Earth Sciences, University of Lausanne, Géopolis, Quartier Mouline, 1015 Lausanne, Switzerland

[3] School of Earth and Environmental Sciences, University of Portsmouth, Portsmouth PO1 3QL, UK

[4] School of Geography, Earth and Environmental Sciences, Plymouth University, Plymouth PL4 8AA, UK

the Southern Alps, the Ivrea Zone represents a tilted cross section through the lower continental crust of the Adriatic margin (e.g., Mehnert 1975; Fountain 1976; Quick et al. 1995, 2003). The Ivrea Zone is well known for its Permian magmatism (e.g., Rivalenti et al. 1984; Sinigoi et al. 1994; Peressini et al. 2007; Zanetti et al. 2013; Klötzli et al. 2014) and HT metamorphism. It exposes a continuous metamorphic field gradient from mid-amphibolite to granulite facies conditions (e.g., Schmid and Wood 1976; Zingg 1980; Sills 1984; Redler et al. 2012; Kunz et al. 2014), and *P–T* conditions of regional Permian metamorphism are well constrained (e.g., Henk et al. 1997; Luvizotto and Zack 2009; Redler et al. 2012; Ewing et al. 2013). The timing of HT low-to-medium pressure metamorphism as well as the associated magmatic underplating has been documented by U/Pb zircon and Th-U/Pb monazite age dating (e.g., Vavra et al. 1999; Vavra and Schaltegger 1999; Peressini et al. 2007 and references therein; Ewing et al. 2013). The cooling history has been studied by U/Pb rutile dating (Ewing et al. 2015) as well as Ar/Ar hornblende, K/Ar biotite, and zircon fission-track ages (e.g., Siegesmund et al. 2008). Ewing et al. (2013) showed that U/Pb zircon ages from the Ivrea Zone combined with trace element thermometry (Ti-in-zircon, Zr-in-rutile) provide insight into the *T–t* evolution during the Permian.

Adria-derived slices of continental crust in the Western Alps (Sesia-Dent Blanche nappes and external klippen) also preserve evidence for Permian metamorphism. Especially where Alpine metamorphic overprint is weak, such as in the Seconda Zona Dioritico Kinzigitica (2DK) and Valpelline Series (Fig. 1), pre-Alpine HT assemblages are often visible in the field and have been confirmed in thin sections (e.g., Carraro et al. 1970; Vuichard 1987; Manzotti and Zucali 2013). This led Carraro et al. (1970) to assign the 2DK and Valpelline Series to a single nappe originating from the Ivrea Zone. Where the Alpine HP metamorphic overprint is strong (in internal parts of the Sesia Zone and in external klippen), only local relics of pre-Alpine metamorphism are preserved (e.g., Lardeaux and Spalla 1991). In the Dent Blanche nappe, Permian HT metamorphism has been dated using zircon and monazite between 300–260 Ma (e.g., Zucali et al. 2011; Manzotti et al. 2012). However, at a regional scale, age data for the Permian HT metamorphic event are lacking so far, whereas Permian magmatism is well documented from gabbroic and granitic intrusives (e.g., Paquette et al. 1989; Bussy et al. 1998; Rubatto et al. 1999; Monjoie et al. 2007; Cenki-Tok et al. 2011). No temporal relations of the metamorphism in Adria-derived units of the Western Alps have been established so far, nor is it clear what age span the metamorphic imprint across all of the units in the Western Alps may be, or how comparable the duration of the HT low-to-medium pressure imprint is to the Southern Alps. These space–time relations are relevant to understand the early stages of extension at the Adriatic margin. In the future, the age pattern may serve to constrain the original crustal position of continental fragments now exposed in the Sesia-Dent Blanche nappes and in external klippen units. Therefore, we investigated the age and regional distribution of Permian HT metamorphism in the units of the Western Alps that contain Adria-derived lower continental crust.

Zircon is an optimal tool for this purpose, as it can preserve robust information on the early evolution of polyphase rocks. To relate the zircon U/Pb age data to metamorphic conditions, we used mineral assemblages and relics, the internal textures of zircon, Ti-in-zircon thermometry, and Zr-in-rutile thermometry. Zircon grains typically display complex internal zoning; hence, single growth zones were selected for in situ U/Pb dating of zircon by LA-ICP-MS. To ensure sufficient amounts of zircon and to simplify comparison within and between data sets, clastic metasediments (mostly metapelites) and leucosomes were analysed. The extent and distribution of Permian metamorphism in continental units from the Western Alps are documented below for 17 select samples from the Sesia Zone (12 from the 2DK, five from the Eclogitic Micaschist Complex), five from the Valpelline Series in the Dent Blanche nappe, and three from the Mt. Emilius Klippe.

## Geological setting

### Western Alps

The internal Western Alps comprise oceanic and continental units. They result from the large-scale continental collision between two or three continental domains, i.e., Europe, Iberia (Briançonnais), and Adria (Pfiffner 2009; Handy et al. 2010). The oceanic units involved are remnants of the Jurassic to Cretaceous Piemonte-Liguria Ocean. The Sesia-Dent Blanche nappes and the Mt. Emilius Klippe represent continental units derived from the northwest margin of Adria; they mainly comprise slices of Palaeozoic basement rocks that underwent subduction and exhumation since the Upper Cretaceous, and hence, they were strongly metamorphosed and deformed during Alpine orogeny. Information on their pre-Alpine history is but sporadically preserved. The Sesia-Dent Blanche nappes represent the highest tectonic elements in the Western Alps, thrusted onto the oceanic units. They comprise the Sesia Zone, the Dent Blanche Tectonic System, and the Pillonet Klippe. A comprehensive view of the tectonometamorphic evolution of the Sesia-Dent Blanche nappes was recently published by Manzotti et al. (2014a). The main characteristics of the Sesia-Dent Blanche nappes and the Mt. Emilius Klippe are briefly

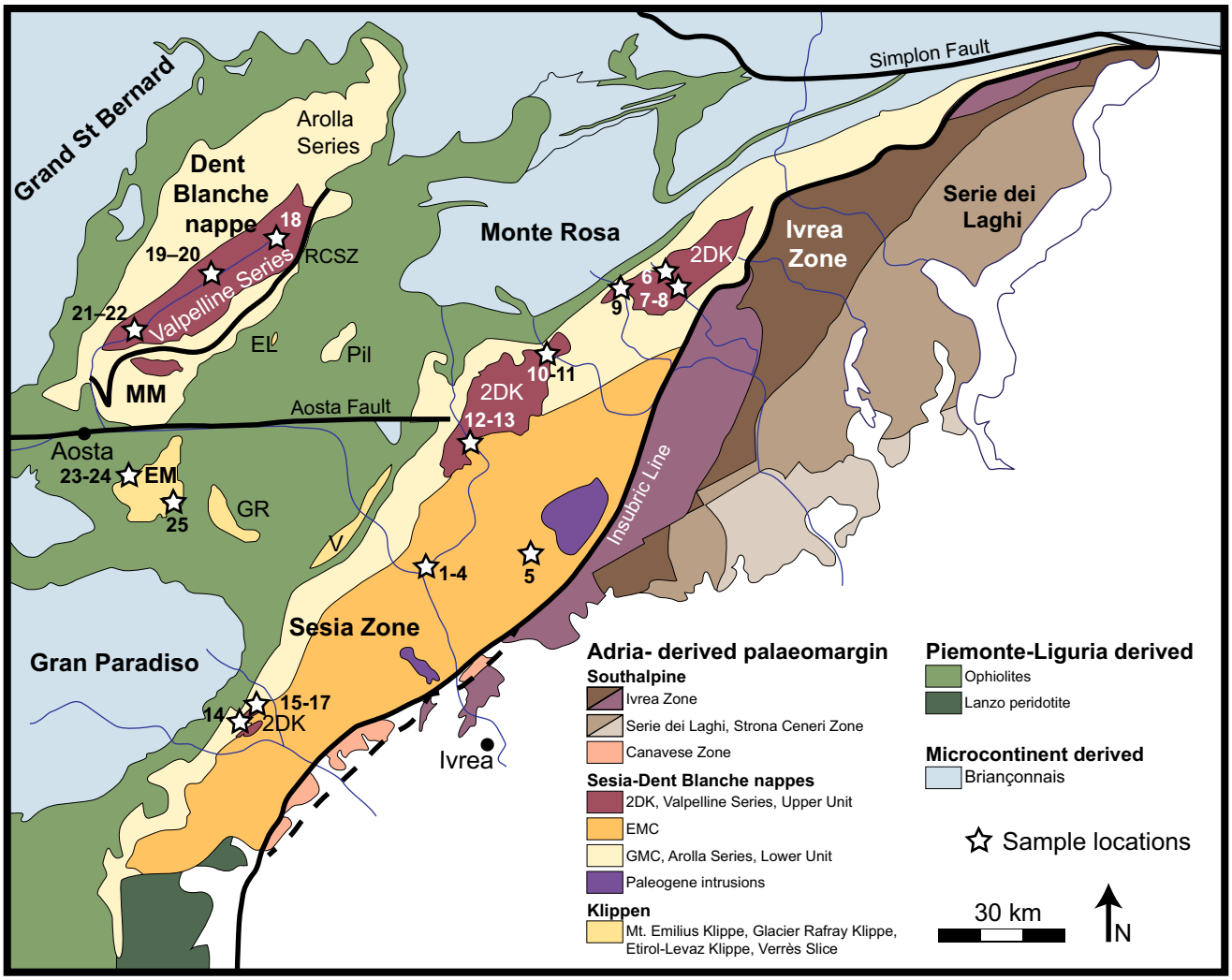


**Fig. 1** Geological overview map of the Western and Southern Alps. Sample localities are indicated by *stars* with numbers corresponding to Table 1. The South-Alpine domain is subdivided into the Ivrea Zone representing lower continental curst levels and the Serie dei Laghi/Strona-Ceneri Zone, which originate from middle to upper crustal levels. The Ivrea Zone is further subdivided into the Mafic Complex in purple and the Kinzigite Formation in dark brown. The Serie dei Laghi/Strona-Ceneri Zone is subdivided into middle crustal rocks in medium brown and light brown for upper crustal sediments and volcanics. *2DK* Seconda Zona Dioritico Kinzigitica; *EL* Etirol-Levaz Klippe; *EM* Mt. Emilius Klippe; *EMC* Eclogitic Micaschist Complex; *GMC* Gneiss Minuti Complex; *GR* Glacier Rafray Klippe; *MM* Mont Mary nappe; *Pil* Pillonet Klippe; *RCSZ* Roisan Cignana Shear Zone; *V* Verrès Slice. Map based on Bousquet et al. (2012) and Bigi and Carrozzo (1990)

reviewed here, highlighting the pre-Alpine evolution of these units.

## Sesia Zone

The Sesia Zone is classically divided into three sub-units: (i) the Eclogitic Micaschist Complex (EMC), (ii) the Seconda Zona Dioritico Kinzigitica (2DK), and (iii) the Gneiss Minuti Complex (GMC) (e.g., Compagnoni et al. 1977), though other subdivisions have been suggested more recently (Babist et al. 2006; Giuntoli and Engi 2016). The EMC and GMC show a strong Alpine metamorphic overprint, whereas the 2DK largely preserves pre-Alpine HT assemblages (e.g., Carraro et al. 1970; Dal Piaz et al. 1971, 1972; Compagnoni et al. 1977; Gosso 1977; Lardeaux et al. 1982; Vuichard 1989; Zucali et al. 2002).

### Eclogitic Micaschist Complex (EMC)

The EMC is the most internal and biggest unit in the Sesia Zone (Fig. 1). It is mostly made of polymetamorphic basement (mostly metasediments, minor metabasites, and metacarbonates) containing derivates of felsic and mafic intrusives; all rock types show a strong and pervasive Alpine

eclogite facies overprint (e.g., Compagnoni et al. 1977; Compagnoni 1977). While the EMC was long regarded as one coherent unit, recent studies (Regis et al. 2014; Giuntoli and Engi 2016) showed that it comprises several tectonic slices with partly diverging Alpine imprint. From various localities, pre-Alpine HT relics (e.g., sillimanite, biotite, garnet, orthoclase) have been reported (e.g., Dal Piaz et al. 1972; Compagnoni 1977; Lardeaux and Spalla 1991; Robyr et al. 2014). Based on such remnants, metamorphic conditions were estimated at 700–800 °C and 8–11 kbar for mafic granulites (Lardeaux et al. 1982) and at 700 °C and 3.5 kbar for sparse amphibolites (Gosso et al. 2010). So far, the age of the pre-Alpine HT metamorphism has not been constrained by radiometric dating. Geochronological studies mostly focused on magmatic rocks, which indicate both Carboniferous (e.g., Ivozio gabbro, 355 ± 9 Ma, Rubatto et al. 1998) and Permian intrusives (Val Sermenza gabbro, 288 +2/-4 Ma, Bussy et al. 1998; Monte Mucrone granitoids, 293 +1/−2 Ma, Paquette et al. 1989; Bussy et al. 1998; Rubatto et al. 1999; Cenki-Tok et al. 2011).

### Seconda Zona Dioritico Kinzigitica (2DK)

Rocks of the 2DK mainly surface as discrete bodies in three parts of the Sesia Zone (see Fig. 1). In the northeast (e.g., Val Mastallone), a coherent body is wedged between the 'Scisti di Fobello e Rimella' (Canavese Zone) and the GMC. In more central parts of the Sesia Zone, between Val Sesia and Val del Lys, another fragment of 2DK is situated between the EMC and the GMC. In the area between Val del Lys and Val Ayas, small discontinuous lenses of reddish schists occur (Giuntoli and Engi 2016), which are assigned to the 2DK (Bertolani 1964; Dal Piaz et al. 1971, 2010; Dal Piaz 1976; Manzotti et al. 2014a, b). Further to the southwest (Pont Canavese area), small lenses of 2DK outcrop along the contact between the GMC and the EMC. The 2DK unit overall comprises mostly metapelites with minor amphibolites, basic granulites, and metacarbonates (e.g., Carraro et al. 1970). In most of the 2DK bodies the dominant metamorphic imprint is upper-amphibolite to granulite facies; however, locally, in shear zones and along tectonic boundaries to adjacent units, an imprint at greenschist/blueschist facies conditions can be pervasive (e.g., Vuichard 1987; Ridley 1989; Pognante et al. 1988; Stünitz 1989). Pre-Alpine metamorphic conditions in the 2DK have been estimated at 700–830 °C and 6–8 kbar (e.g., Vuichard 1987; Pognante et al. 1988). Reliable geochronological constraints on the pre-Alpine history of the 2DK are missing; based on similarities, ages have often been assumed to correspond to those in the Ivrea Zone. Some early studies did date 2DK samples using K/Ar in muscovite (e.g., 177 ± 9 Ma; Hunziker 1974) and Ar/Ar in biotite (e.g., 273–66 Ma; Reddy et al. 1996), but the large range in these results hampers their interpretation.

### Gneiss Minuti Complex (GMC)

The GMC is the most external sub-unit of the Sesia Zone. Rocks of the GMC are mostly greenschist facies orthogneisses with local occurrence of paragneisses and minor calcsilicates (e.g., Compagnoni et al. 1977). It remains a debate whether the GMC reached HP conditions during Alpine times. Some studies reported jadeite relics (Williams and Compagnoni 1983; Spalla et al. 1991), suggesting a minimum pressure of 12 kbar for the Alpine metamorphism of the GMC, but based on detailed mapping (Giuntoli and Engi 2016), the position of these localities is uncertain, and Alpine maximum pressures were likely lower. Pre-Alpine relics in the GMC are rare, although magmatic allanite, K-feldspar, and apatite have been reported for some samples from the GMC (Giuntoli 2016).

### Pillonet Klippe

The Pillonet Klippe, sitting on top of the Piemonte-Liguria oceanic units, lies midway between the external part of the Sesia Zone (GMC) and the Dent Blanche nappe (e.g., Dal Piaz et al. 2001). The Pillonet Klippe is characterised by fine-grained orthogneiss (Permian metagranitoids), paragneisses (Variscan/Permian), metagabbros (Permian), and Mesozoic metasediments including carbonates (e.g., Dal Piaz and Sacchi 1969; Dal Piaz 1976). The Pillonet Klippe preserves evidence of Alpine blueschist facies metamorphism (glaucophane, phengite; Dal Piaz 1976). Ar/Ar data from mica in paragneiss yield Permian ages of 260–253 Ma, whereas Rb/Sr data indicate 310 Ma (Cortiana et al. 1998). U/Pb zircon ages from a leucocratic dyke yield Variscan magmatic ages of 355 ± 4 Ma and 312 ± 5 Ma, while monazite (Th/Pb age: 289 ± 9 Ma) and allanite (Th/Pb age: 266 ± 10 Ma) from the same sample indicate a medium-temperature/low-pressure metamorphic overprint in the Permian (Grossen 2012).

### Dent Blanche Tectonic System

The Dent Blanche Tectonic System (Manzotti et al. 2014b) is the most external Adria-derived continental unit in the Western Alps (Fig. 1), surfacing north of the Aosta-Ranzola fault, resting on top of remnants of the Piemonte-Liguria Ocean. It comprises the Mont Mary nappe and the Dent Blanche nappe, which are separated by a 25 km long Alpine high-strain zone (the Roisan Cignana Shear Zone, Manzotti et al. 2014b). The Mont Mary nappe and the Dent Blanche nappe consist of slices of continental basement rocks, representing sections of late Palaeozoic upper

crust (the Arolla Series in the Dent Blanche nappe and the Lower Unit in the Mont Mary nappe), and lower crust (the Valpelline Series in the Dent Blanche nappe and the Upper Unit in the Mont Mary nappe; e.g., Manzotti et al. 2014a). Remnants of Mesozoic sedimentary cover are represented by the Mont Dolin Series and the Roisan Zone (Ayrton et al. 1982; Manzotti 2011; Ciarapica et al. 2016). The latter unit is strongly deformed and metamorphosed together with basement rocks along the Roisan Cignana Shear Zone. In the Dent Blanche nappe, the Valpelline Series consists of metapelites, metabasites, and metacarbonates with a dominant metamorphic imprint at amphibolite to granulite facies conditions (700–800 °C, 7–9 kbar), the pre-Alpine age of which remains poorly constrained (e.g., Diehl et al. 1952; Nicot 1977; Gardien et al. 1994; Zucali et al. 2011; Manzotti and Zucali 2013). The Alpine imprint, mainly under greenschist facies conditions, is weak and only locally developed (De Leo et al. 1987). Kiénast and Nicot (1971) described Alpine assemblages with kyanite-chloritoid in metapelite, suggesting conditions of 7–8 kbar and ~525 °C for the Alpine evolution. In the Upper Unit of the Mont Mary nappe, Permian metamorphic zircon ages ranging from 294 to 263 Ma have been reported for metasediments from the Valtournenche area (Manzotti et al. 2012). Similarly, in the Valpelline Series, Permian metamorphism has been dated in zircon from a pegmatite (274 ± 1 Ma; Zucali et al. 2011; Manzotti 2012), whereas monazite in a migmatite shows a range from late Carboniferous to early Triassic (304–248 Ma; Zucali et al. 2011; Pesenti et al. 2012). Permian magmatic intrusives are well known in the Dent Blanche Tectonic System, notably from the Collon and Cervino gabbros: 284 ± 1 Ma, ID-TIMS U/Pb zircon crystallisation age (Monjoie et al. 2007); 246 ± 8 Ma, K/Ar and 257 ± 6 Ma, Rb/Sr biotite cooling ages (Dal Piaz et al. 1977). Felsic intrusives such as the Arolla granite yield zircon crystallisation ages of 290 ± 2 Ma and of 294.5 ± 6.0 Ma (LA-ICP-MS, Manzotti 2012), in agreement with an ID-TIMS age of 289 ± 2 Ma for Arolla orthogneiss (Bussy et al. 1998).

### External klippen

Adria-derived continental units form several klippen (Fig. 1) situated between sub-units derived from the Piemonte-Liguria Ocean, specifically below the Combin zone and on top of the Zermat-Saas zone (e.g., Dal Piaz 1976, 1999; Ballèvre et al. 1986). The two largest of these outliers are the Mt. Emilius Klippe and the Glacier–Rafray Klippe, both situated south of the Aosta-Ranzola fault. They comprise pre-Alpine basement rocks (metapelites, -basites, -granites, and carbonates) overprinted by Alpine eclogitic metamorphism and locally retrogressed at greenschist facies conditions (e.g., Dal Piaz and Nervo 1971; Dal Piaz et al. 1983). Evidence of pre-Alpine metamorphism in the Mt. Emilius Klippe is preserved as mineral relics (e.g., garnet, rutile, and zircon), and *P–T* conditions for HT metamorphism have been estimated to 700–750 °C at maximum pressure of 6–8 kbar (Dal Piaz et al. 1983). The only constraints on the age of pre-Alpine metamorphism for the Mt. Emilius Klippe are based on Rb/Sr whole rock data; these yield ages of ~450 Ma (Hunziker 1974). Granitic intrusives gave early Permian zircon crystallisation ages of 293 ± 3 Ma (Bussy et al. 1998).

## Analytical methods

All sample preparation and analytical work was done at the Institute of Geological Sciences, University Bern. Rock samples were disaggregated using a Selfrag Lab system. Zircon was separated by classical heavy mineral separation, hand picked, mounted in acryl/epoxy, and polished to equatorial section. CL-images were made using a ZEISS EVO 50 scanning electron microscope. Electron microprobe analysis on rutile was performed on polished thin sections with a JEOL JXA8200. Measurements for zircon U/Pb-geochronology and trace elements were performed by LA-ICP-MS using a GeoLas-Pro 193 nm ArF Excimer laser system (Lambda Physik) combined with an Elan DRC-e quadrupole mass spectrometer (Perkin Elmer). Detailed analytical protocols are reported in the Online Resource 1. U and Th concentrations were measured during geochronological and during trace element analysis, and concentrations reported here and discussed are the data obtained during geochronology measurements as they represent the same sample volume as the U/Pb dates. The term date refers to individual $^{206}Pb/^{238}U$ spot analyses, while the term age is used for groups of $^{206}Pb/^{238}U$ dates that are regarded as geologically significant.

## Sample description

The present study emphasises mineral assemblages and relics associated with Permian HT metamorphism. Other mineral phases not related to HT metamorphism in part reflect post-Permian retrogression or Alpine metamorphism. In some units, such as in the EMC, southwestern parts of the 2DK, and the Mt. Emilius Klippe, the Alpine metamorphism was pervasive, and its products can be identified with confidence. However, in the northeastern and central parts of the 2DK and in the Valpelline Series, the generations often cannot be distinguished unambiguously. Sample localities (Fig. 1) and further information (e.g., GPS position, mineral assemblages, and main metamorphic imprint) for each sample are given in Table 1. Mineral abbreviations

**Table 1** List of samples investigated in this study

| | Sample | Lithology | Coordinates | | Locality | Mineral assemblage | preserved HT Mineral assemblage | Main meta-morphic imprint |
|---|---|---|---|---|---|---|---|---|
| ***EMC*** | | | | | | | | |
| **1** | FG 1249 | Metasediment | 406555 | 5053733 | Faye, Val del Lys | *Ph+Pg+Qtz+Grt+Aln/Ep/Czo+Rt+Gln/Ab/Amp+Zrn* | **Grt+Mnz+Zrn** | HP |
| **2** | FG 12157 | Metasediment | 409601 | 5053835 | Lillianes, Val del Lys | *Ph+Qtz+Grt+Gln+Ep/Czo/Aln+Chl+Ab+Rt/Ttn/Ilm+Gr+Zrn* | **Grt+Zrn** | HP |
| **3** | FG 1315 | Metasediment | 408432 | 5051382 | Vers-Vert, Val del Lys | *Qtz+Ph+Pg+Grt+Aln/Czo+Chl+Ab/Amp+Rt+Gr+Zrn* | **Grt+Mnz+Zrn** | HP |
| **4** | FG 1347 | Metasediment | 406236 | 5052276 | Liévanere, Val d'Aosta | *Qtz+Ph+Cld+Grt+Rt+Ep/Czo/Aln+Zrn* | **Grt+Mnz+Zrn** | HP |
| **5** | ROMu-1 | Metasediment | 342369 | 4984896 | Laghetto del Monte Rosso | *Qtz+Wm+Grt+Omph+Chl+Ep+Rt+Gr+Zrn* | **Zrn** | HP |
| ***2DK NE*** | | | | | | | | |
| **6** | IIDK 27a | Metapelite | 430295 | 5084906 | A. Piana sup., Val Mastallone | *Grt+Wm+Qtz+Pl**+Kfs**+Sil**Bt**+Czo+Chl+Zrn+Mnz+Ap+Rt+Ilm* | **Grt+Qtz+Pl+Kfs+Sill+Bt+Zrn+Ap+Rt+Ilm** | HT |
| **7** | IIDK 52c | Leucocratic dyke | 433590 | 5084239 | St. Maria, Val Mastallone | *Qtz+Pl+Kfs+Wm+Grt+Bt**+Ep/Czo+Chl+Mnz/Ap/Aln+Rt*+Zrn+Ilm* | **Qtz+Pl+Kfs+Grt+Bt+Chl+Mnz+Rt+Zrn+Ilm** | HT |
| **8** | IIDK 54 | Metapelite | 432651 | 5084613 | St. Maria, Val Mastallone | *Grt+Qtz+Wm+Bt+Pl*+Kfs*+Sil+Rt+Ilm+Czo/Ep+Cdt+Zrn+Mnz* | **Grt+Qtz+Bt+Pl+Kfs+Sil+Rt+Ilm+Zrn+Mnz** | HT |
| **9** | IIDK 17 | Metapelite | 426778 | 5083943 | Carcoforo, Val d'Egua | *Qtz+Wm+Chl+Grt**+Rt+Zrn* | **Qtz+Grt+Rt+Zrn** | GS |
| ***2DK central*** | | | | | | | | |
| **10** | IIDK 01 | Metapelite | 417964 | 5075679 | Riva Valdobbia, Val Sesia | *Qtz+Wm+Grt+Chl+Pl*+Kfs*+Bt**+Czo/Ep+Zrn+Ttn+Ilm+Py+Gr* | **Qtz+Wm+Grt+Pl+Kfs+Bt+Zrn+Ilm+Py+Gr** | HT |
| **11** | IIDK 03 | Leucosome | 417964 | 5075679 | Riva Valdobbia, Val Sesia | *Qtz+Wm+Grt+Pl*+Bt**+Chl+Czo/Ep+Zrn+Ttn+Gr* | **Qtz+Wm+Grt+Pl+Bt+Zrn+Gr** | HT |
| **12** | IIDK 65 | Metapelite | 410936 | 5065094 | Pont Trenta, Val del Lys | *Qtz+Wm+Grt+Pl*+Kfs*+Bt**+Chl+Czo/Ep+Zrn+Mnz+Ttn+Gr* | **Qtz+Wm+Grt+Pl+Kfs+Bt+Zrn+Mnz+Gr** | HT |
| **13** | IIDK 66 | Leucosome | 410936 | 5065094 | Pont Trenta, Val del Lys | *Qtz+Grt+Wm+Pl**+Bt**+Chl+Czo/Ep+Zrn+Mnz+Ttn* | **Qtz+Grt+Wm+Pl+Bt+Zrn+Mnz** | HT |
| ***2DK SW*** | | | | | | | | |
| **14** | VR 0909 | Metapelite | 385658 | 5032740 | Vasario, Valle di Ribordone | *Qtz+Grt+Wm+Gln+Pl+Rt+Zrn+Gr+Chl+Czo+Ilm+Ttn* | **Qtz+Grt+Pl+Rt+Zrn+Gr+Ilm** | BS |
| **15** | VS 1009 | Metapelite | 387843 | 5035282 | Ingria, Val Soana | *Pl+Qtz+Wm+Czo+Chl+Ttn+Zrn+Ep+Ap+Aln+Rt* | **Pl+Qtz+Zrn+Ap+Rt** | GS |
| **16** | VS 1015 | Leusosome | 388319 | 5035497 | Ingria, Val Soana | *Wm+Qtz+Czo+Grt+Gln+Pl+Zrn+Aln/Ap/Mnz+Chl+Stpn+Rt* | **Qtz+Grt+Pl+Zrn+Mnz+Rt** | GS |

**Table 1** continued

| | Sample | Lithology | Coordinates | | Locality | Mineral assemblage | preserved HT Mineral assemblage | Main meta-morphic imprint |
|---|---|---|---|---|---|---|---|---|
| **17** | VS 1017 | Leusosome | 388319 | 5035497 | Ingria, Val Soana | *Qtz+Wm+Grt+Bt+Czo+Pl+Ttn+Rt+Ap+Amp+Aln+Zrn* | **Qtz+Grt+Bt+Pl+Rt+Ap+Zrn** | GS |
| ***Valpelline Series*** | | | | | | | | |
| **18** | VP 1402 | Metapelite | 383420 | 5084284 | Lac des Places de Moulin | *Qtz+Grt+Bt+Wm+Pl*+Chl+Kfs*+Czo/Ep+Zrn+Rt* | **Qtz+Grt+Bt+Wm+Pl+Kfs+Zrn+Rt** | HT |
| **19** | VP 1403a | Restite | 376288 | 5080408 | Bionaz, Valpelline | *Grt+Bt+Sil+Pl+Zrn+Chl+Rt* | **Grt+Bt+Sil+Pl+Zrn+Rt** | HT |
| **20** | VP 1403b | Leucosome | 376288 | 5080408 | Bionaz, Valpelline | *Qtz+Pl+Kfs+Wm+Czo/Ep+Zrn+Cc+Rt* | **Qtz+Pl+Kfs+Wm+Zrn+Rt** | HT |
| **21** | VP 66 | Metapelite | 372874 | 5077575 | Thoules, Valpelline | *Pl+Sil+Bt+Qtz+Grt+Rt+Ms+Ep+Zrn+Rt* | **Pl+Sil+Bt+Qtz+Grt+Rt+Ms+Zrn+Rt** | HT |
| **22** | VP 74 | Metapelite | 372874 | 5077575 | Thoules, Valpelline | *Grt+Bt+Pl+Qtz+Sil+Rt+Ms+Ep+Chl+Zrn+Rt* | **Grt+Bt+Pl+Qtz+Sil+Rt+Ms+Zrn+Rt** | HT |
| ***Mt. Emilius Klippe*** | | | | | | | | |
| **23** | EM1-1049 | Metasediment | 372990 | 5060520 | Becca di Nona | *Qtz+Grt+Wm+Gln+Czo+Chl+Rt+Zrn+Ttn* | **Grt+Rt+Zrn** | HP |
| **24** | EM1-1051 | Metasediment | 372990 | 5060520 | Becca di Nona | *Qtz+Grt+Wm+Chl+Gln+Czo/Ep+Rt+Zrn+Ttn* | **Grt+Rt+Zrn** | HP |
| **25** | EM1-1056 | Metasediment | 374747 | 5056999 | Laghi di Lussert | *Qtz+Wm+Grt+Gln+Rt+Zrn+Ap* | **Grt+Rt+Zrn** | HP |

* partially replaced; ** completly replaced

follow Kretz (1983) and migmatite terminology Sawyer (2008).

### Eclogitic Micaschist Complex (EMC)

The samples from the EMC (Fig. 1) are micaschists with a pervasive Alpine eclogite facies imprint; assemblages (Table 1) comprise white mica (phengite and paragonite), quartz, garnet, epidote, and rare glaucophane and clinozoisite. Accessory phases are allanite, rutile, titanite, graphite, and ilmenite. Sample FG 1347 additionally preserves chloritoid, and sample ROMu-1 has omphacite. Strong Alpine deformation and a HP metamorphic overprint erased most macroscopic evidence of pre-Alpine metamorphism. At the micro-scale, isolated mineral relics remain, notably as cores of garnet porphyroblasts and zircon, very sparsely monazite occurs as well. In none of the micaschist samples, we studied a more complete record of the pre-Alpine metamorphic HT evolution preserved, but coronitic domains in other lithotypes of the EMC have been reported (e.g., Zucali 2011) from some areas.

### Seconda Zona Dioritico Kinzigitica (2DK)

In the field, the samples from most 2DK bodies (Fig. 1) show evidence of pre-Alpine HT metamorphism and partial melting, based on their mineral assemblages, coarse grain size, and separation of leucosome and melanosome domains (see Fig. 2). Near contacts to the EMC or the GMC, the 2DK rocks show an Alpine blueschist to greenschist facies overprint. Permian HT metamorphic assemblages (Table 1) include garnet, biotite, sparse sillimanite, plagioclase, K-feldspar, quartz, and local rutile. Accessory phases associated with the HT assemblage are mostly zircon, monazite, apatite, ilmenite, and graphite. Retrogression is marked by chlorite replacing biotite and garnet, white mica and epidote/clinozoisite replacing plagioclase, and monazite showing coronas of apatite and allanite. The samples from the SW 2DK additionally contain Alpine glaucophane, albite, and titanite. In sample, IIDK 54 biotite shows exsolution of very fine rutile needles, and small, pale green aggregates of chloritoid and amphibole reveal retrogression or a low-grade overprint. Alpine metamorphic overprint increases from absent to minor in the NE 2DK, to a faint greenschist facies overprint in the central 2DK, and a strong greenschist to blueschist facies overprint in the SW 2DK.

### Valpelline Series

Samples from the Valpelline Series of the Dent Blanche nappe were collected along the Valpelline valley (Fig. 1; Table 1). All samples show field evidence indicating HT metamorphism and partial melting, such as a coarse grain size, migmatite textures, distinct leucosome, and melanosome domains (Fig. 2). In thin section, pre-Alpine HT assemblages including garnet, biotite, plagioclase, K-feldspar, sillimanite, muscovite, and quartz are well preserved. Zircon, rutile, monazite, apatite, ilmenite, and graphite are the most common accessory phases associated with the HT assemblage. Manzotti and Zucali (2013) estimated (peak) *P–T* conditions of 814 ± 40 °C and 6–8 kbar for samples VP 66 and VP 74. Sericite, epidote/clinozoisite, and chlorite indicate Alpine retrogression.

### Mt. Emilius Klippe

The three samples from the Mt. Emilius Klippe are from two localities (see Fig. 1; Table 1). The metasediments sampled show reddish weathering and a layered appearance. All three samples show Alpine HP overprint and variable greenschist retrogression. They are dominated by the HP assemblage white mica, garnet, quartz, chlorite, glaucophane, and clinozoisite with accessory titanite, allanite, and rutile. Minerals retaining information about pre-Alpine metamorphism are cores of large garnet porphyroblasts, dark brown/red rutile grains (>200 µm), and zircon.

## Zircon

### Zircon textures

All samples in our study contain zircon, but the quantity, quality (ideally clear, not fractured and non-metamict), and grain size vary from sample to sample. The samples from the EMC show a large variability, some have abundant grains of good quality and grain sizes up to 100–200 µm, while other samples only contain few (<20) grains of poor quality and small grain sizes (<70 µm). The metapelites from the 2DK, Valpelline Series, and the Mt. Emilius Klippe usually have sufficient quantities of good quality zircon with grain sizes up to 200 µm. The highest amount of high-quality zircon with grain size up to 500 µm was found in leucosomes from the 2DK and Valpelline Series. Representative CL-images of zircon are shown in Fig. 3. The samples from the EMC mostly have short-prismatic zircon (Fig. 3a–d), while zircon from the 2DK, Valpelline Series, and Mt. Emilius Klippe often shows roundish shapes (Fig. 3e–s). In some, samples (e.g., leucosome) of these units crystals with (short) prismatic habit are also present (Fig. 3i). The internal morphology of zircon crystals varies from sample to sample, even from grain to grain in some samples. Many samples preserve detrital cores, with one or several metamorphic overgrowth zones, while other samples show newly grown Permian metamorphic

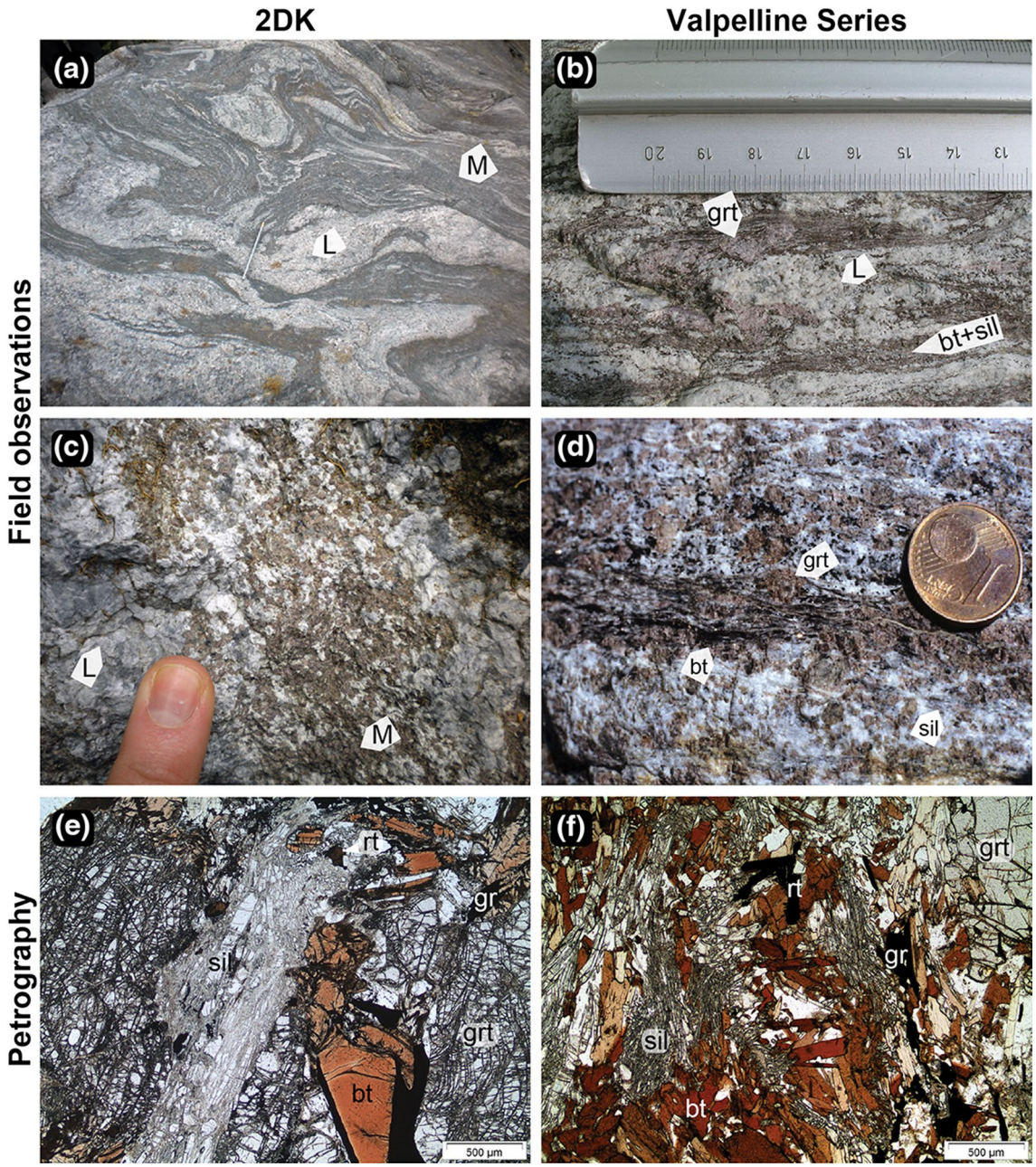


**Fig. 2** Selected field and thin section photographs representative for the high-grade metasediments from the 2DK and Valpelline Series. **a** Migmatite typical of the central 2DK, with distinct leucosome (L) and melanosome (M) domains. **b** Migmatite from the Valpelline Series; L domains interlayered with garnet, biotite, and sillimanite schlieren. **c** L-rich migmatite with garnet, sillimanite, and biotite in M from the 2DK. **d** Garnet-rich migmatite from the Valpelline Series with schlieren of intergrown biotite and sillimanite. **e** Thin section photomicrograph from a M/restite (2DK) with large garnet porphyroclasts, surrounded by dark red biotite and prismatic sillimanite; rutile crystals are typically abundant in restitic parts of these migmatites. **f** Thin section photomicrograph from the Valpelline Series with garnet porphyroclasts surrounded by intergrown prismatic sillimanite and red Ti-rich biotite

zircon only. Internal textures within detrital cores are diverse, but oscillatory zoning is the most common type. A first very narrow metamorphic overgrowth usually has a bright CL-emission, a turbulent texture, and many inclusions (Fig. 3e, m); however, such a bright rim is not present (or not preserved) in all grains. The most common type of metamorphic overgrowth has a dark-CL-emission with either uniform texture, sector, or fir-tree zoning (e.g., 3b-d, e, g-l, o–s). In addition, some migmatite samples from the 2DK, Valpelline Series, and Mt. Emilius Klippe commonly show oscillatory zoning (Fig. 3n). A fourth Permian metamorphic overgrowth rim is present in some samples; it

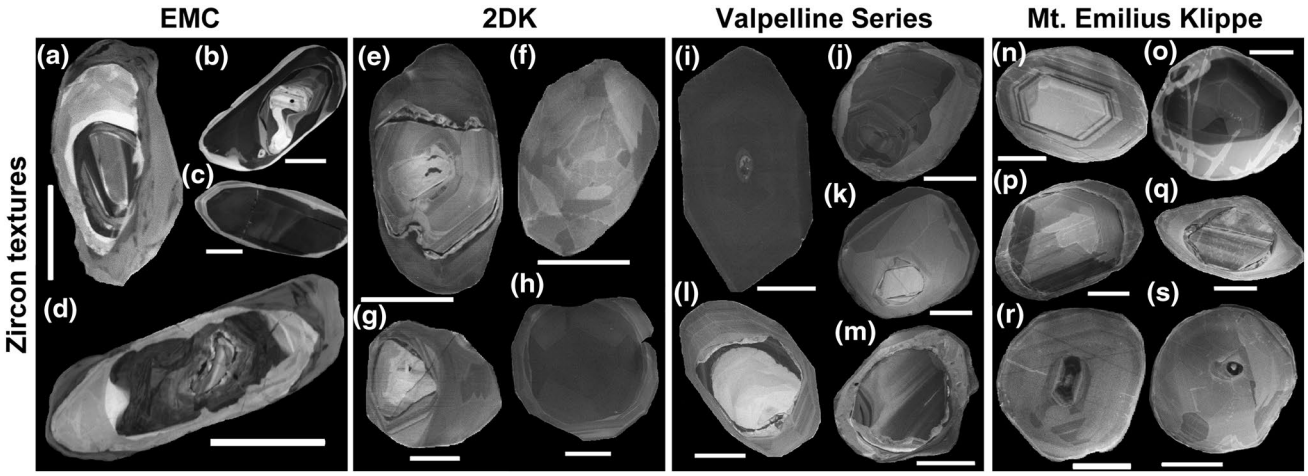


**Fig. 3** Select representative zircon CL-images of metapelites except of grain (**h**), which originates from a grt-leucosome. **a–d** Complex zoned zircon from the EMC with detrital cores, overgrown by up to two Permian rims (CL-dark, CL-bright) and Alpine overgrowth for **a** and **d**. **e–h** Zircons representative for the samples from the 2DK. Some samples/grains preserve detrital cores **e**, **g**, while others consist of newly grown metamorphic zircon only **f**, **h**. **i–m** Zircon from the Valpelline Series with partially to completely resorbed detrital cores and at least two generation of Permian metamorphic overgrowth. **n–s** Typical zircon textures from the samples of the Mt. Emilius Klippe. Some grains show mostly detrital cores with thin metamorphic overgrowth **p**, **q**, while other samples show mostly metamorphic growth and non-relic or relic cores only **n**, **o**, **r**, **s**. *Scale bar* in all images corresponds to 50 µm. A detailed description of the zircon texture for each image is given in the Online Resource 2

shows very bright CL-emission and a mostly uniform texture (Fig. 3a–d, j, o). Samples from the EMC (FG 12157, FG 1315, FG 1347) also show an Alpine metamorphic zircon overgrowth (outermost grey rim in Fig. 3a, d).

## U/Pb-geochronology

Table 2 gives an overview of the range in Permian and detrital U/Pb zircon dates, uranium and thorium concentration, and Th/U ratios, as well as weighted mean ages for each sample. Figure 4 shows probability density plots (PDP) for individual samples, while Fig. 5 shows PDP for the six units. The full data set with individual analyses is given in the Online Resource 6; only concordant $^{206}Pb/^{238}U$ dates are reported in all tables. A representative selection of CL-images with location of LA-ICP-MS measurement spots is given in Online Resource 5. Weighed mean ages and unmixing ages have been calculated with Isoplot v4.15 (Ludwig 2003).

In the five EMC samples analysed, 17 detrital cores give a range of dates from 790 to 415 Ma, and 53 metamorphic rims range from 313 to 222 Ma (Fig. 4a). In samples from the northeastern 2DK, 16 zircon cores show a range of dates between 1000–500 Ma, and 106 analyses of metamorphic overgrowth rims yield an overall range between 311–217 Ma (Fig. 4b). In the central 2DK body, 16 detrital cores yield a range from 1800 to 450 Ma, and 63 metamorphic overgrowth rims have a range from 329 to 266 Ma (Fig. 4c). For the 2DK slices in the southwest Sesia Zone, five analyses of detrital cores define a range of dates from 560 to 352 Ma, 79 dates of metamorphic overgrowth rims range from 305 to 259 Ma (Fig. 4d). Five samples from the Valpelline Series yield 13 analyses of partially resorbed cores, with dates ranging from 1500 to 350 Ma; 75 analyses of metamorphic rims range from 330 to 230 Ma (Fig. 4e). In the samples from the Mt. Emilius Klippe, 19 analyses of detrital cores yield dates from 900 to 450 Ma, and 29 analyses for metamorphic rims range overall from 327 to 264 Ma (Fig. 4f).

All Permian dates (see Fig. 5) from the EMC combined form a broad peak in the PDP, spanning from 300 to 280 Ma with a maximum at ~285 Ma, giving a weighted mean age (WMA) of 285.9 ± 2.7 Ma ($n = 46$; MSWD = 2.9). A similar range is observed in the central 2DK (main peak ~286 Ma; WMA: 285.8 ± 1.9 Ma, $n = 55$, MSWD = 2.5), Mt. Emilius Klippe (main peak ~285 Ma; WMA: 285.7 ± 2.2 Ma, $n = 22$, MSWD = 1.4), and one of two peaks from the Valpelline Series (~283 Ma; Isoplot unmix age: 283.5 ± 1.7 Ma). The data from the SW 2DK show a broad range of dates with several unresolved peaks in PDP at ~286 Ma, ~280 Ma and ~270 Ma (Isoplot unmix ages: 287.3 ± 1.5 Ma, 278.4 ± 2.0 Ma, 268.6 ± 1.8 Ma). The dates from the NE 2DK form a well-defined peak at ~277 Ma (WMA: 277.0 ± 1.1 Ma; $n = 103$, MSWD = 1.9) falling in-between the older peak (286–283 Ma) and the younger peak of the Valpelline Series at ~266 Ma (Isoplot unmix age: 265.6 ± 1.8 Ma). Few dates from the EMC, NE 2DK, and Valpelline Series scatter towards younger ages between 260–220 Ma.

**Table 2** Summary table of U/Pb ages, Th-, U-, concentration and Th/U ratios in zircon

| | | Permian dates | | | | | | | Detrital core dates | | |
|---|---|---|---|---|---|---|---|---|---|---|---|
| | Sample | # analyses | Max (Ma) | Min (Ma) | Weighted mean age | U (ppm) | Th (ppm) | Th/U | # detrital core analyses | Max (Ma) | Min (Ma) |
| ***EMC*** | | | | | | | | | | | |
| **1** | FG 1249 | 5 | 300±17 | 277±15 | **294.2±2.8 Ma** (MSWD=0.89; n=11); **279.5±2.3 Ma** (MSWD=1.14; n=13) | 326–868 | 2–5 | 0.003–0.014 | 11 | 793±20 | 414±17 |
| **2** | FG 12157 | 24 | 302±14 | 268±16 | **285±11 Ma** (MSWD=1.3; n=5) | 121–1781 | 2–28 | 0.007–0.044 | – | – | – |
| **3** | FG 1315 | 12 | 313±13 | 222±13 | **285.8±5.6 Ma** (MSWD=0.39; n=6) | 167–1478 | 1–5 | 0.002–0.01 | 6 | 696±50 | 353±25 |
| **4** | FG 1347 | 9 | 299±21 | 247±11 | **295.7±7.6 Ma** (MSWD=0.068; n=5) | 126–1112 | 0.3–8 | 0.002–0.012 | – | – | – |
| **5** | ROMu-1 | 3 | 303±14 | 290±11 | **297±16 Ma** (MSWD=1.4; n=3) | 148–1722 | 0.7–15 | 0.005–0.009 | – | – | – |
| ***2DK NE*** | | | | | | | | | | | |
| **6** | IIDK 27a | 17 | 310±12 | 268±13 | **279.4±3.4 Ma** (MSWD=2.0; n=14); **302.6±5.8 Ma** (MSWD=1.08, n=3) | 156–2050 | 5–311 | 0.017–0.296 | 7 | 786±26 | 364±14 |
| **7** | IIDK 52c | 59 | 293±16 | 267±6 | **276.3±1.1 Ma** (MSWD=1.3; n=59) | 133–664 | 35–316 | 0.115–0.550 | – | – | – |
| **8** | IIDK 54 | 26 | 311±14 | 266±8 | **285.3±2.7 Ma** (MSWD=0.53; n=16); **271.1±2.8 Ma** (MSWD=0.54; n=9) | 214–1881 | 26–170 | 0.056–0.366 | 9 | 955±41 | 544±15 |
| **9** | IIDK 17 | 4 | 287±11 | 217±7 | – | 195–295 | 67–104 | 0.246–0.399 | – | – | – |
| ***2DK central*** | | | | | | | | | | | |
| **10** | IIDK 01 | 5 | 303±7 | 289±5 | **301.7±4.4 Ma** (MSWD=0.12; n=2); **289.4±3.3 Ma** (MSWD=0.102; n=3) | 304–729 | 4–8 | 0.009–0.012 | 9 | 978±20 | 346±5 |
| **11** | IIDK 03 | 11 | 310±12 | 284±9 | **290.7±4.6 Ma** (MSWD=2.1; n=11) | 105–1260 | 0.5–20 | 0.005–0.035 | 5 | 1877±95 | 485±17 |
| **12** | IIDK 65 | 25 | 293±13 | 266±6 | **278.7±3.2 Ma** (MSWD=4.2; n=25) | 393–7800 | 5–34 | 0.003–0.025 | 2 | 930±40 | 516±22 |
| **13** | IIDK 66 | 22 | 329±13 | 272±15 | **289.4±3.4 Ma** (MSWD=1.5; n=20) | 316–1609 | 3–69 | 0.006–0.065 | 1 | 563±23 | – |

**Table 2** continued

| | | Permian dates | | | | | | | Detrital core dates | | |
|---|---|---|---|---|---|---|---|---|---|---|---|
| | Sample | # analyses | Max (Ma) | Min (Ma) | Weighted mean age | U (ppm) | Th (ppm) | Th/U | # detrital core analyses | Max (Ma) | Min (Ma) |
| ***2DK SW*** | | | | | | | | | | | |
| **14** | VR 0909 | 15 | 290±12 | 260±13 | **271.7±4.4 Ma** (MSWD=2.1; n=15) | 57–109 | 26–85 | 0.456–0.819 | 3 | 451±16 | 311±10 |
| **15** | VS 1009 | 10 | 282±13 | 268±9 | **277.3±3.1 Ma** (MSWD=0.98; n=10) | 42–109 | 20–72 | 0.41–0.667 | – | – | – |
| **16** | VS 1015 | 23 | 306±7 | 260±8 | **302.9±3.1 Ma** (MSWD=0.35; n=4); **282.8±4.8 Ma** (MSWD=8; n=18) | 259–403 | 25–111 | 0.076–0.426 | 3 | 557±9 | 380±10 |
| **17** | VS 1017 | 32 | 290±9 | 262±7 | **278.4±2.8 Ma** (MSWD=8; n=32) | 104–359 | 34–142 | 0.274–0.491 | – | – | – |
| ***Valpelline Series*** | | | | | | | | | | | |
| **18** | VP 1402 | 7 | 313±11 | 285±11 | **288.0±3.9 Ma** (MSWD=0.31; n=6) | 237–3524 | 22–176 | 0.043–0.123 | 6 | 672±24 | 435±11 |
| **19** | VP 1403a | 16 | 285±17 | 260±16 | **273.7±4.1 Ma** (MSWD=0.64; n=16) | 317–1056 | 13–259 | 0.015–0.5 | – | – | – |
| **20** | VP 1403b | 26 | 298±18 | 270±16 | **280.5±2.4 Ma** (MSWD=2.8; n=26) | 296–2219 | 8–77 | 0.019–0.082 | – | – | – |
| **21** | VP 66 | 13 | 297±8 | 257±6 | **289.1±6.3 Ma** (MSWD=1.4; n=5); **262.7±3.9 Ma** (MSWD=1.9; n=8) | 206–393 | 21–88 | 0.079–0.259 | 5 | 507±17 | 346±14 |
| **22** | VP 74 | 13 | 330±15 | 230±9 | **263.9±3.0 Ma** (MSWD=1.4; n=9) | 79–881 | 13–108 | 0.04–0.621 | 2 | 1604±84 | 1073±46 |
| ***Mt. Emilius Klippe*** | | | | | | | | | | | |
| **23** | EM1-1049 | 12 | 327±7 | 278±8 | **284.9±3.5 Ma** (MSWD=1.7; n=8) | 121–455 | 11–144 | 0.03–0.403 | 2 | 932±19 | 606±12 |
| **24** | EM1-1051 | 10 | 295±7 | 271±13 | **286.5±5.4 Ma** (MSWD=1.7; n=10) | 165–735 | 1–22 | 0.005–0.134 | 11 | 903±21 | 455±12 |
| **25** | EM1-1056 | 7 | 297±10 | 264±10 | **282.6±5.2 Ma** (MSWD=0.015; n=4) | 123–730 | 7–76 | 0.012–0.398 | 6 | 880±32 | 496±22 |

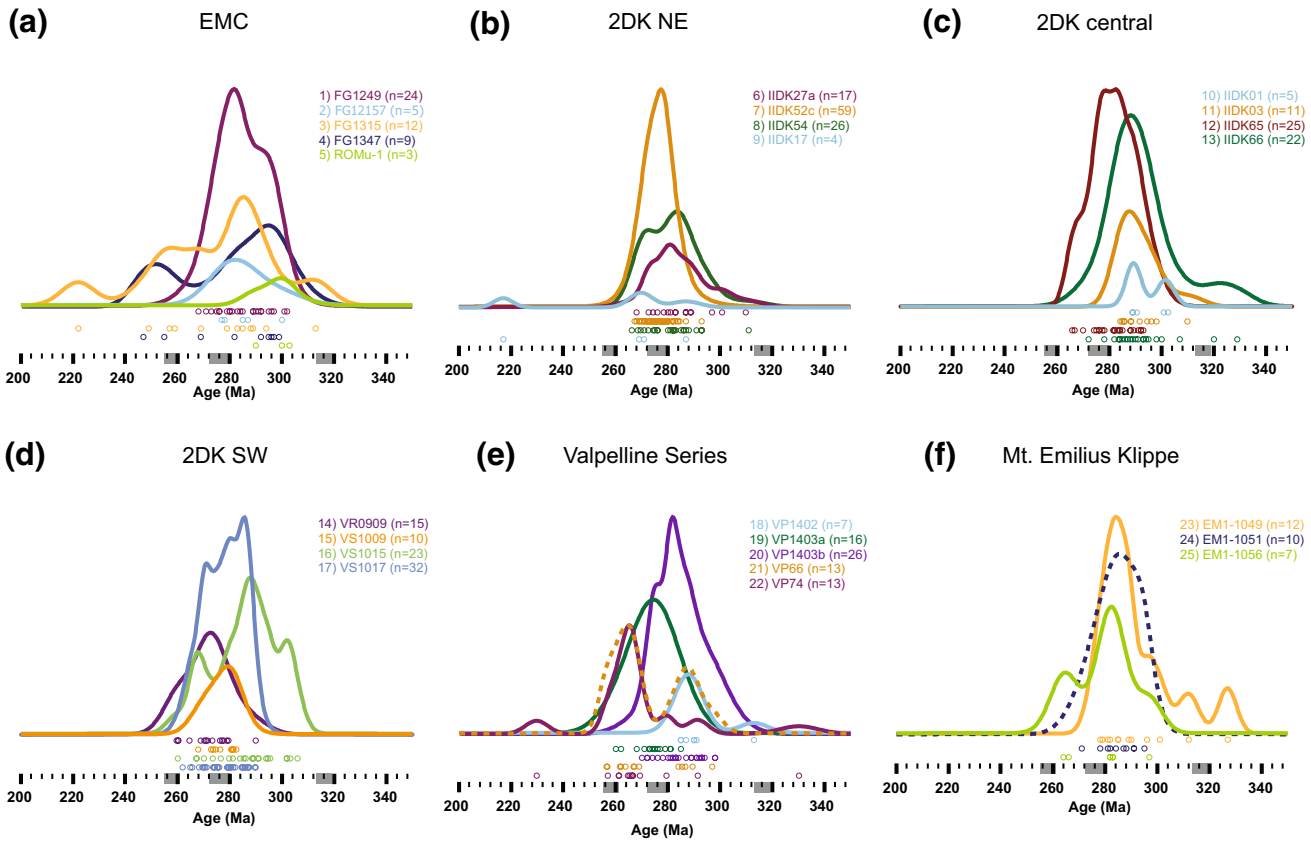


**Fig. 4** Probability density plots for U/Pb zircon dates for individual samples from: **a** EMC, **b** 2DK NE, **c** 2DK central, **d** 2DK SW, **e** Valpelline Series, and **f** Mt. Emilius Klippe. Individual rock samples are colour-coded; *n* number of age data. The individual lines are scaled to their relative abundance of analysed to give more weight to curves with more data points

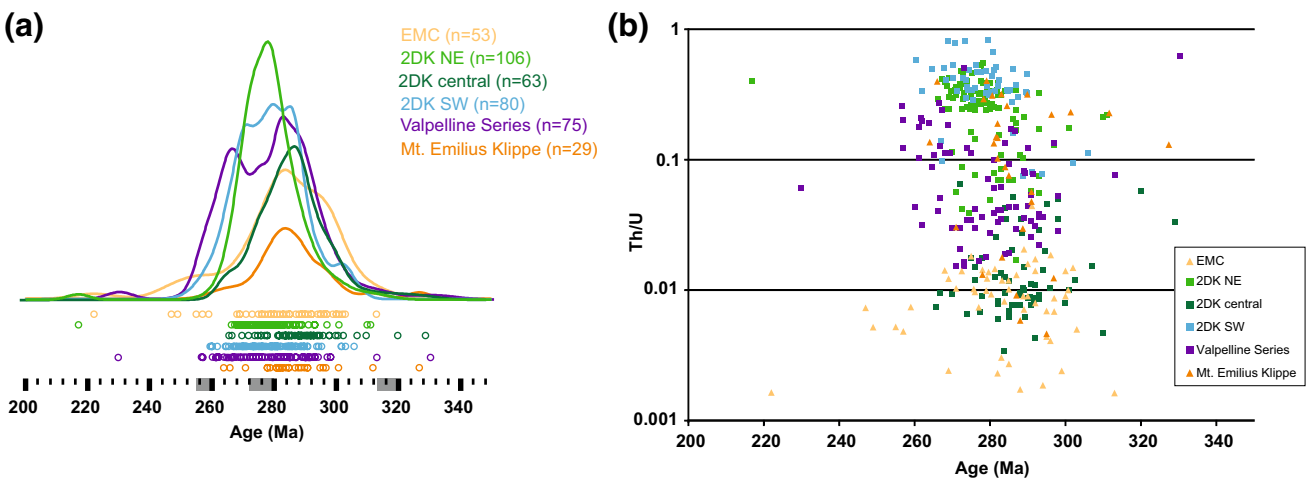


**Fig. 5** **a** Probability density plots showing the combined geochronological results for all samples. **b** Th/U ratios plotted against their U/Pb zircon age. *Square symbols* indicate samples with no to limited HP-overprint; *triangle symbols* indicate samples with pervasive HP-overprint

**Table 3** Summary table of Ti-in-zircon and Zr-in-rutile thermometry

| | Sample | Ti-in-Zrn concentration (ppm) | Ti-in-Zrn temperature (°C) | Zr-in-Rt concentration (ppm) | Zr-in-Rt temperature (°C) |
|---|---|---|---|---|---|
| ***EMC*** | | | | | |
| **1** | FG 1249 | 2.0–2.8 | 618–641* | 4–288 | 385**–639** |
| **2** | FG 12157 | – | – | – | – |
| **3** | FG 1315 | – | – | – | – |
| **4** | FG 1347 | – | – | – | – |
| **5** | ROMu-1 | – | – | – | – |
| ***2DK NE*** | | | | | |
| **6** | IIDK 27a | 8.6–15.1 | 727–778 | – | – |
| **7** | IIDK 52c | 6.3–14.6 | 707–776 | – | – |
| **8** | IIDK 54 | 4.3–11.0 | 672–749 | 563–2186 | 690–840 |
| **9** | IIDK 17 | 14.0–25.1 | 771–829 | – | – |
| ***2DK central*** | | | | | |
| **10** | IIDK 01 | 2.2–3.8 | 624–662* | – | – |
| **11** | IIDK 03 | 1.2–4.0 | 581–666* | – | – |
| **12** | IIDK 65 | 2.3–4.4 | 628–673* | – | – |
| **13** | IIDK 66 | 1.7–10.5 | 607–745* | – | – |
| ***2DK SW*** | | | | | |
| **14** | VR 0909 | 19.7–43.1 | 804–888 | 571–2035 | 700–830 |
| **15** | VS 1009 | 3.7–7.8 | 660–720 | – | – |
| **16** | VS 1015 | 2.3–7.8 | 627–720 | – | – |
| **17** | VS 1017 | – | – | – | – |
| ***Valpelline Series*** | | | | | |
| **18** | VP 1402 | 3.8–7.8 | 662–719 | – | – |
| **19** | VP 1403a | 4.8–7.3 | 679–714 | – | – |
| **20** | VP 1403b | 2.9–6.4 | 642–703 | – | – |
| **21** | VP 66 | 2.6–13.5 | 635–768 | 400–2395 | 665–850 |
| **22** | VP 74 | 4.1–10.1 | 669–741 | 346–2049 | 630–830 |
| ***Mt. Emilius Klippe*** | | | | | |
| **23** | EM1-1049 | 4.8–10.6 | 680–746 | – | – |
| **24** | EM1-1051 | – | – | 10–1190 | 432**–770 |
| **25** | EM1-1056 | 11.5–25.9 | 753–832 | – | – |

*minimum temperature; no rutile present

**alpine resetting

## Zircon trace element geochemistry

Thorium and uranium concentration were routinely analysed with the U/Pb data (Table 3; Online Resource 6). For select samples from the 2DK and Valpelline Series, trace elements (P, Y, Hf, and REE) were separately analysed (Online Resource 6). Th/U ratios of Permian zircon from the EMC and central 2DK (Fig. 5b) are generally low ~0.01–0.001, while high Th/U ratios >0.1 prevail in the NE and SW 2DK. Permian zircon from the Valpelline Series and Mt. Emilius Klippe shows a range of Th/U ratios from 0.01 to >0.1. In the Valpelline Series, there is an apparent trend for higher Th/U ratios with younger ages (Fig. 5b).

LREE and MREE patterns of Permian zircon from the 2DK and Valpelline Series broadly overlap for all samples, while HREE patterns show variation within and/or between samples. Two major groups can be distinguished: (i) steep HREE slopes with $Gd_N/Lu_N$ of 3–30 and (ii) flat to slightly negative HREE slopes with $Gd_N/Lu_N$ between 0.4–2. Zircon from leucosome samples (IIDK 52c, IIDK 66, and VR1015) generally fall into the first group of steep HREE pattern and have overall uniform REE pattern within their zircon population. Zircon from metapelitic samples

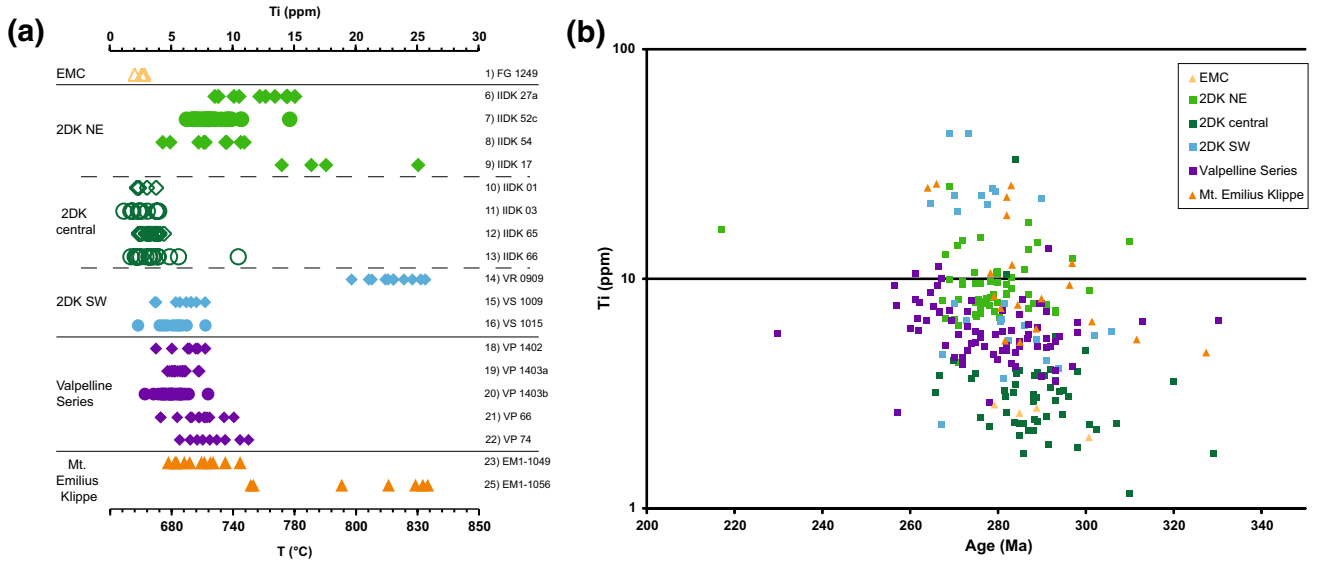


**Fig. 6** **a** Ti concentration in zircon, with corresponding Ti-in-zircon temperatures shown (calibration of Watson et al. 2006). **b** Ti-in-zircon concentration plotted against U/Pb age. *Diamond symbols* metapelites; *circle symbols* leucosome; *triangle symbols* HP-overprinted samples; *closed symbols* rutile present; *open symbols* presence of rutile is unclear or absence

mostly shows a significant variation in their HREE pattern within each sample ($Gd_N/Lu_N$ 0.4–30), except of sample VR 0909, which has overall flat and uniform HREE patterns ($Gd_N/Lu_N$ 0.62–1.54). Only in one sample (VP 66) from the Valpelline Series, a clear correlation of HREE patterns and ages has been found; steep HREE slopes ($Gd_N/Lu_N$ 12–123) are associated with older ages (284–297 Ma), while flat slopes are present in the age generation around 260 Ma. A negative Europium anomaly is present in all Permian zircon (Eu/Eu* 0.03–0.44).

## Ti-in-zircon thermometry

Titanium concentration in zircon were measured by LA-ICP-MS either simultaneously with U/Pb measurements or as part of trace element measurements (for detailed analytical protocols see Online Resource 1). Temperatures were calculated using the calibration from Watson et al. (2006). Except where stated otherwise, all samples contain rutile and quartz, but in some samples, all rutile may be Alpine. The data presented are associated with Permian metamorphic zircon rims; an overview for each sample is given in Table 3 and Fig. 6; the Online Resource 6 shows individual analyses. Where rutile was absent during zircon growth, the $TiO_2$ activity was reduced, and temperatures represent minimum values. Ti-in-zircon concentrations range from a few ppm in the central 2DK (1–4 ppm) and EMC (2–3 ppm), to 5–15 ppm in most samples of the NE and SW 2DK, Valpelline Series, and Mt. Emilius Klippe. Three samples (IIDK 17, VR 0909 and EM1-1056) show very high concentration (>25 ppm). In most samples from the EMC and one from the Mt. Emilius Klippe (EM1-1051),

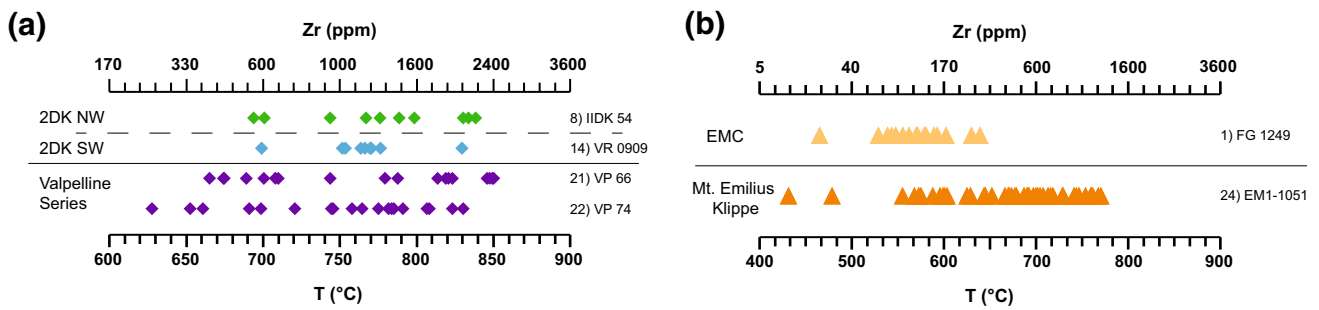


**Fig. 7** Zr concentration in rutile with corresponding Zr-in-rutile temperatures (calibration of Watson et al. 2006; zircon is present in all samples). **a** Zr-in-rutile for samples with little to no Alpine overprint from the NE and SW 2DK, as well as the Valpelline Series. **b** Zr-in-rutile for samples with strong Alpine metamorphic overprint from the EMC and Mt. Emilius Klippe. *Diamond symbols* metapelites; *triangle symbols* HP-overprinted samples

growth zones are narrow, requiring a small spot for LA-ICP-MS analysis. As Ti concentration in these samples was low, they were below detection limit (<3 ppm). For the EMC (FG 1249) Ti concentrations could be measured only in one sample. Due to the strong Alpine metamorphic overprint in EMC samples, it is not possible to be sure whether rutile and/or ilmenite were part of the HT assemblage, and hence, the Ti-in-zircon concentration (2–3 ppm) and temperatures (618–641 °C) derived from FG 1249 are minimum values. Except for a few outliers, Permian zircon from the NE 2DK shows high (4.3–15.1 ppm) Ti concentrations. In all samples from that unit rutile is present and considered part of the HT assemblage, the data translate to Ti-in-zircon temperatures of ~680–780 °C for Permian growth. In the central 2DK, all measured Ti-in-zircon concentrations for Permian zircon rims are low (<5 ppm except for one outlier). In these samples, rutile was found only as exsolution needles in biotite. Due to the notable greenschist facies overprint, we are unsure if rutile was present during Permian HT metamorphism. The ~580–680 °C obtained for the central 2DK are thus considered minimum temperatures for the Permian metamorphism. The samples from the southwestern 2DK show that two contrasting ranges, VS 1009 and VS 1015, have low to intermediate Ti concentrations (2.3–7.8 ppm) in their Permian zircon growth zones. On the other hand, sample VR 0909 retains very high Ti concentrations (~20–40 ppm). Despite a relatively strong greenschist to blueschist facies overprint, rutile can be found, and we consider it part of the HT assemblage in the samples from the SW 2DK. Based on this, the distinct Ti-in-zircon concentrations are thought to represent real differences in temperature (~627–888 °C) during Permian zircon growth. Ti concentrations increase from low (3.8–7.8 ppm) in sample VP 1402 towards higher values (2.6–13.5 and 4.1–10.0 ppm) in samples VP 66 and VP 74. In all samples from the Valpelline Series, rutile is present, and Ti-in-zircon temperatures ranging from 642 to 768 °C are likely to represent zircon growth during Permian HT metamorphism. In two samples from the Mt. Emilius Klippe, for which Ti-in-zircon data could be acquired, Ti concentrations similarly dispersed as in the samples from the SW 2DK, ranging from 4.8 to 10.6 ppm in sample EM1-1049, and 11.5–25.9 ppm in sample EM1-1056. Despite a strong Alpine metamorphic overprint in the samples from the Mt. Emilius Klippe, evidence for rutile belonging to the HT assemblage is present, and Ti-in-zircon temperatures of 680–832 °C are indicated for Permian zircon growth.

## Zr-in-rutile thermometry

Zr-in-rutile concentrations were measured by electron microprobe; for detailed analytical conditions and protocols, see supplementary material Online Resource 1. Rutile is present in many samples, but fresh HT rutile was found only in a few samples that allowed Zr-in-rutile measurements for the calculation of temperatures to be warranted. The range of Zr concentration and temperatures, calculated using the Watson et al. (2006) calibration, are listed in Table 3 and plotted in Fig. 7. Individual analyses for the six measured samples together with a selection of BSE images from the analysed rutile grains are given in Online Resources 5 and 6.

In HT assemblages, rutile is commonly dark red to brown, and crystals are up to 700 µm in diameter. In the samples from the EMC no large, dark HT rutile grains could be found. Instead, rutile in these samples is small (10–150 µm) and usually of light brown to yellow colour. Zr concentrations were measured in one sample from the EMC (FG 1249) to test if rutile Zr contents were reset during Alpine HP overprint. Indeed, Zr concentrations in this sample range from 4 to 288 ppm, corresponding to temperatures of 385–639 °C, clearly cooler than the Permian metamorphism in the 2DK and Valpelline Series. In the northeastern 2DK, rutile is very common, but occasionally replaced in part by ilmenite and/or titanite and/or showing exsolution of µm-sized zircon/baddeleyite needles. Fresh rutile was found in sample IIDK 54. Avoiding areas showing replacement or exsolution, the sample yields Zr concentrations of 563–2186 ppm, corresponding to temperatures of ~690–840 °C. In samples from the central 2DK lens, no HT rutile was found. Occasionally, very fine rutile needles occur in exsolution textures in HT biotite. Owing to the strong greenschist facies overprint in the southwestern 2DK, fresh rutile is rare, but in sample VR 0909, some rutile grains were unaffected by ilmenite and/or titanite replacement. These have a range in Zr concentration of 571–2035 ppm, i.e., a temperature range of ~700–830 °C, similar to the northeastern 2DK. Samples from the Valpelline Series commonly show abundant fresh HT rutile. Two samples (VP 66 and VP 74) where selected for Zr measurements. Both data sets show a slightly larger spread than in the 2DK samples, with Zr concentrations of 400–2395 ppm (~665–850 °C) for sample VP 66 and 346–2049 ppm (~630–830 °C) for VP 74. For samples from the Mt. Emilius Klippe, despite strong Alpine overprint, some pre-Alpine rutile grains are preserved. Sample EM1-1051 shows dark brown rutile grains, locally overgrown or rimmed by fine-grained, lighter coloured rutile grains, and small, separate light brown to yellow rutile is also found. Rutile grains of all sizes and colours were analysed for Zr concentrations resulting in a range from 10 to 1190 ppm (432–770 °C). The lowest Zr concentrations were found in the rims of some grains, while the highest usually were found in the centre. However, some low values were from inside dark brown rutile grains, indicating

reset Zr concentrations in rutile without textural/microscopic evidence. For the Mt. Emilius Klippe samples, the calculated Zr-in-rutile temperatures ranging from ~620 to 770 °C are thought to reflect Permian HT metamorphism; the results overlap closely with those for the 2DK and Valpelline Series. Temperatures ranging from 430 to 600 °C are similar to those inferred to represent Alpine temperatures in the sample from the EMC (Fig. 7b). The diversity of the Zr concentration in rutile from the Mt. Emilius Klippe indicates several generations of rutile growth and partial resetting of Zr in HT rutile.

## Discussion

In the Alps, HT metamorphism has long been related to the late Variscan orogenic evolution (e.g., Schmerold 1988; Desmons et al. 1999 and references therein; Frisch and Neubauer 1989; Neubauer et al. 1989; Gardien et al. 1994) and associated with thermal relaxation in the overthickened lithosphere and late-orogenic collapse. Owing to Alpine overprint, the age of this metamorphism is largely assumed to be coeval to the magmatic evolution, which mostly spans a range from 340 to 295 Ma (e.g., Bussy et al. 2000; Online Resource 4). Over the past two decades, studies in late Palaeozoic metamorphic rocks increasingly recognised a distinct Permian thermal phase, which has variably been associated with upwelling of the asthenospheric mantle, mafic underplating, and continental rifting (e.g., Diella et al. 1992; Bertotti et al. 1993; Müntener and Hermann 2001; Marotta and Spalla 2007; Schuster and Stüwe 2008). For the Eastern Alps, crustal-scale extensional processes in the course of the separation of Europe and Adria are now thought to be responsible for the LP-HT Permian metamorphism (e.g., Schuster et al. 2001a). A similar Permian extensional evolution, characterised by a high thermal regime, has been proposed also for the Western Alps (e.g., Lardeaux and Spalla 1991; Marotta and Spalla 2007; Schuster and Stüwe 2008; Beltrando et al. 2007), but such a separate Permian evolution was so far supported mostly by geochronological data from magmatic rocks (i.e., Permian gabbros and granitoids; e.g., Paquette et al. 1989; Bussy et al. 1998; Bussy and Cadoppi 1996; Rubatto et al. 1999; Bertrand et al. 2005; Monjoie et al. 2007; Cenki-Tok et al. 2011); overall, these indicate an age group (mostly 290–270 Ma; Fig. 9; Online Resource 3) distinct from the late Variscan one. An HT metamorphic imprint of Permian age has long been assumed, but geochronological data to support this idea have been few and far between (e.g., Zucali et al. 2011; Manzotti, 2012; Pesenti et al. 2012). The present study fills this gap by adding age data of Permian metamorphic rocks from the Western Alps, in particular from Adria-derived tectonic units. The overall age range spans a time interval of 40–50 Myr in the Permian, indicating that HT metamorphism in the continental crust was protracted and, indeed, defines a separate group than the late-orogenic Variscan one.

### Zircon U/Pb age interpretation

Zircon grains dated in this study were separated from metasediments, mostly metapelites, i.e., from samples that are expected to have behaved similarly under comparable metamorphic conditions. In addition, garnet-bearing leucosome veins or dykes were selected from some units (2DK and Valpelline Series). In many samples, zircon shows crystal habits ('soccer-ball' shaped; Fig. 3g, h, k, o, r, s; c.f. Vavra et al. 1996, 1999) and internal textures that indicate growth at HT metamorphic conditions (dark-CL, uniform, sector, or fir-tree zoning; Fig. 3c, f, h, i, j, s) or in anatectic environments (oscillatory zoning; Fig. 3l, n, r) (e.g., Harley et al. 2007). Analytical spots for dating of metamorphic growth of zircon were chosen based on such textural criteria.

To discuss the spatial–temporal evolution regionally, it is useful to distinguish two sample domains: Domain A comprises the EMC, central 2DK, and Mt. Emilius Klippe; domain B includes the NE 2DK, SW 2DK, and the Valpelline Series.

U/Pb zircon dates ranging from ~310 to 260 Ma are found all over domain A and B, attesting the regional extent of late Palaeozoic HT metamorphism in the Adria-derived units (shown in Fig. 9, discussed below). The data presented in the PDP of Fig. 4 and 5a show that the overall distribution of dates is scattered among samples and units; however, Fig. 5a shows that pooling of ages allows us to distinguish between age groups among the units. Two main age groups of metamorphic zircon growth are distinguished in both domains (Fig. 5a): the first one (~290–280 Ma) is coeval with or only slightly younger than the Permian magmatism (~294 and ~284 Ma) reported for the Western Alps; the second group (~277–266 Ma) is clearly younger.

In domain A, the first age group dominates the zircon population (Fig. 5a), it has a weighted mean age of 286 ± 2 Ma. In the EMC and central 2DK, this age group is generally associated with low Th/U ratios (Fig. 5b) and low Ti-in-zircon concentration (Fig. 6b), but no such trend is evident in the data from the Mt. Emilius Klippe. In many samples from these three areas, Permian metamorphic overgrowths are narrow, and detrital cores dominate the zircon grains (Fig. 3). Textures indicate limited zircon dissolution and minor new growth during HT metamorphism, possibly because fluid/melt supply was limited or the heat pulse short-lived, thus not allowing a large quantity of zircon to dissolve or grow during the Permian.

In domain B, the first age group is also present (SW 2DK: 287 ± 2 Ma, Valpelline Series: 283 ± 2 Ma; Figs. 4, 5a), but it is the second age group (~277–266 Ma) that dominates the zircon population. The first age group in domain B lacks the characteristics of low Th/U and Ti concentration (Figs. 5b, 6b) and growth zones are wider than in domain A. Whereas a distinct peak is found in the PDP for the NE 2DK, with a weighted mean age of 277 ± 1 Ma (Fig. 5a), no clear age peak emerges for the SW 2DK (Figs. 4d, 5a), just a range of ages that may comprise unresolved peaks. Using Isoplot's unmixing age function, three age generations emerge at 287 ± 2, 278 ± 2, and 268 ± 2 Ma that do correspond to the peaks discernible in the PDP. The Valpelline Series shows a bimodal age distribution with two incompletely separated peaks (Fig. 5a). The Isoplot unmixing age function yields an age at 283 ± 2 Ma and a younger generation at 266 ± 2 Ma. The results indicate that the NE and SW 2DK and Valpelline Series experienced a first zircon growth phase as well as a second one some ~10–20 Myr later. In domain B, metamorphic overgrowth dominates most of the zircon grains, whereas core remnants dominate in Domain A. In domain B HT conditions evidently lead to more resorption either because of higher metamorphic conditions and/or longer duration of these conditions. Extensive partial melting, visible as migmatites, leads to significant zircon resorption followed by new growth over ~20 Myr. Samples in all of domain B show HT metamorphic assemblages, high Th/U ratios in zircon (0.01–0.8; Fig. 5b), and zircon textures indicating growth at amphibolite to granulite facies conditions (Fig. 3f; fir-tree and sector zoning; c.f., Vavra et al. 1996, 1999). Attempts to discriminate different growth phases based on (H)REE patterns (e.g., Rubatto 2002) were inconclusive: HREE slopes vary significantly between steep and flat among and within samples, and no correlation to age, Th/U ratios, Ti-in-zircon temperatures, or textures is evident. This may indicate local processes in small-scale domains, such are expected if partial melts migrate through compositionally heterogeneous rocks.

Age differences are evident also among individual samples. Migmatite parts sampled in close proximity, both in the 2DK (e.g., melanosome IIDK 65; leucosome IIDK 66) and Valpelline Series (melanosome VP 1403a; leucosome VP 1403b), show differences in their age distribution (Fig. 4c, e). Compared to melanosomes, leucosomes tend towards older ages indicating that bulk rock chemistry and/or melt depletion have an influence on apparent ages. Yet, in other studies (e.g., Rubatto et al. 2001), the age difference between leucosome and melanosome was inverse, the leucosome being slightly younger than the melanosome. Yakymchuk and Brown (2014) concluded that apparent age differences between individual samples are most likely caused where migmatites reach the solidus at different temperatures because of differences in local bulk rock composition and/or melt depletion.

Zircon in domain A is characterised by an age of 286 ± 2 Ma, generally low Th/U ratios, low Ti concentration, and narrow Permian metamorphic growth zones. In contrast zircon of domain B shows two age groups (~287–283 and ~277–266 Ma), with high Th/U ratios in zircon, high Ti concentration, and wide Permian metamorphic overgrowths rims. The reasons for these differences cannot unambiguously be identified. A possibility is that domain A and B experienced different duration and intensity of partial melting during HT metamorphism. Therefore, in domain B, more pre-existing zircon has been dissolved and subsequent wider metamorphic rims grew. The varying width of Permian metamorphic growth zones could also explain the difference in age pattern that we observed. Due to the spot size during LA-ICP-MS measurements 32–16 µm, we bias our results towards growth zones at least slightly wider than our spot size. Therefore, the absence or limited number of dates between 277–266 Ma in domain A might not imply that they do not exist; they simply could not be measured.

Scattered younger ages (<260 Ma) are associated with zircon internal textures that indicate late stage fluid-assisted recrystallisation (Fig. 3a, d, o; c.f. SCA, Vavra et al. 1999). Such textures occur in both domains; most abundantly, they are observed in EMC samples (Fig. 5a), but they are locally present in samples from the NE 2DK and Valpelline Series, as well. The age of such recrystallisation events is difficult to specify: they may immediately follow the Permian HT metamorphism or at a later time, perhaps in the Alpine cycle.

## Significance and interpretation of zircon and rutile trace element thermometry

In our study, the temperature ranges from both thermometers are similar (~600–800 °C, Fig. 6, Table 3 and 750–850 °C, Fig. 7, Table 3). The lowest Ti-in-zircon temperatures (600–650 °C) are considered minimum values, as rutile is lacking in some samples and $TiO_2$ activity may have been reduced (e.g., Watson et al. 2006). On the other hand, the high temperatures (>750–800 °C) in sample IIDK 17, VR 0909 and EM1-1056 may reflect local heat anomalies, possibly caused by proximal heat sources such as mafic dykes or intrusive stocks. BSE images of some rutile grains from the EMC, 2DK, and Mt. Emilius Klippe do show exsolution of zircon/baddeleyite needles, but not in samples from the Valpelline Series. Nevertheless, Zr-in-rutile temperatures from the 2DK (690–840 °C) overlap

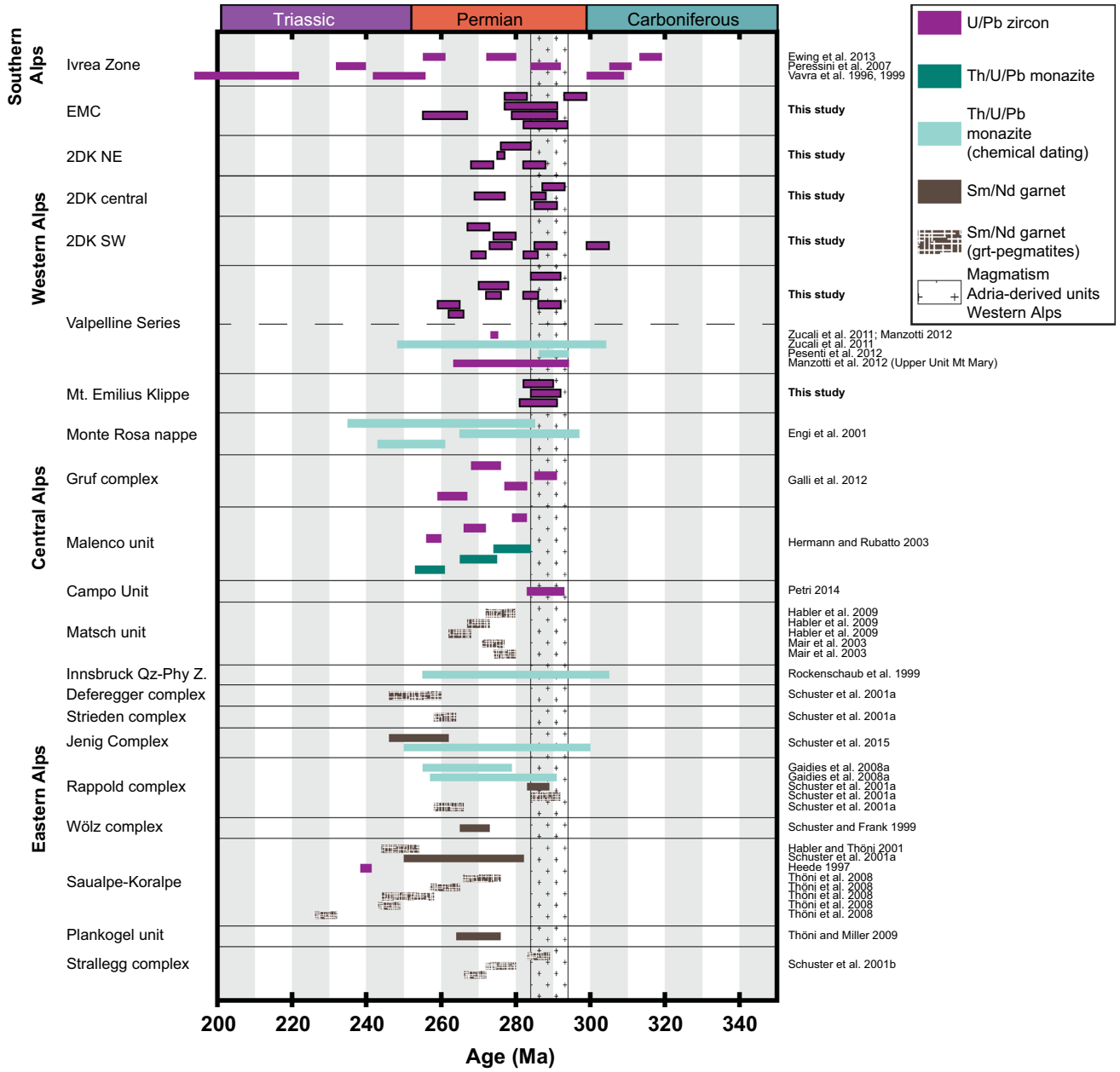


**Fig. 8** Summary of Permian metamorphic ages from the Alps

with those from the Valpelline Series (630–850 °C), so Zr-in-rutile temperatures appear not to be reset. For the EMC and Mt. Emilius Klippe, clearly lower Zr-in-rutile temperatures (385–639 and 432–770 °C) were measured, and these appear to reflect retrogression.

While Ti-in-zircon temperatures in HT rocks commonly are found to be below peak temperatures and may indicate zircon growth during cooling (e.g., Roberts and Finger 1997; Baldwin et al. 2007; Harley 2008) Zr-in-rutile temperatures are interpreted to record metamorphic peak temperatures (e.g., Ewing et al. 2013). Zr-in-rutile temperatures from this study, therefore, suggest that metamorphic peak temperatures did not exceed 800–850 °C in Adria-derived units. The results from trace element thermometry are in good agreement with the *P–T* data from the previous studies, ranging from ~700 to 800 °C at ~6–9 kbar (e.g., Nicot 1977; Lardeaux 1981; Lardeaux et al. 1982; Dal Piaz et al. 1983; Vuichard 1987; Pognante et al. 1988; Lardeaux and Spalla 1991; Gardien et al. 1994; Manzotti and Zucali 2013).

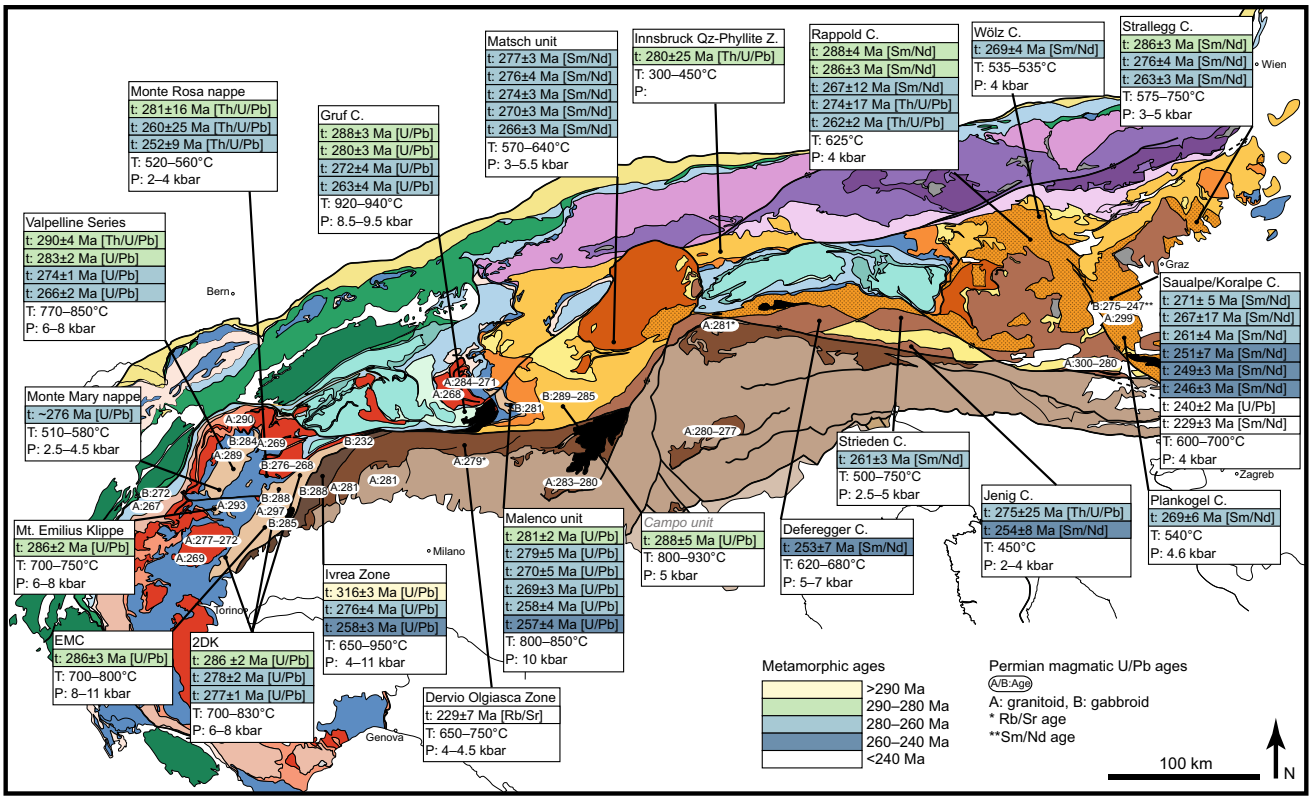


**Fig. 9** Tectonic overview map of the Alps (Schmid et al. 2004) showing *P–T–t* data for Permian metamorphism. References to data presented on the map are given in the text and Online Recourses 3. *Italics* indicate verified contact metamorphism related to magmatic intrusion

## Permian metamorphic ages in the Alps

So far, few geochronological studies focused on unravelling the age of the HT metamorphism in Adria-derived units of the Western Alps. Recent studies in the Valpelline Series provided a Permian U/Pb zircon age from a pegmatite dyke (274 ± 1 Ma; Zucali et al. 2011; Manzotti 2012) and chemical (EMPA) monazite ages from migmatites (304–248 Ma; Zucali et al. 2011 and 290 ± 4 Ma; Pesenti et al. 2012). In addition, Manzotti et al. (2012) obtained metamorphic U/Pb zircon ages, ranging from 294 to 263 Ma, for a metachert from the Upper Unit in the Mont Mary nappe. These sparse age data indicated a prolonged Permian HT metamorphism for the lower crustal units of the Dent Blanche nappe. The new results presented here affirm the Permian age of HT metamorphism in that unit and document comparable ages in the other Adria-derived lower crustal units studied, i.e., the EMC, 2DK, and Mt. Emilius Klippe. Furthermore, the data set as a whole clearly indicates that zircon growth occurred in two distinct time intervals of the protracted HT history of these units. The first age group (290–280 Ma) is contemporaneous with the several known, magmatic ages from the Sesia-Dent Blanche nappes (~294 and ~284 Ma; e.g., Val Sermenza gabbro, Collon and Cervino gabbros, Monte Mucrone granitoids, and Arolla granitoid; e.g., Paquette et al. 1989; Bussy et al. 1998; Rubatto et al. 1999; Monjoie et al. 2007; Cenki-Tok et al. 2011; Manzotti 2012). The second age group clearly postdates that intrusive phase by some 10–20 Myr (see Fig. 8). Three questions emerge:

1. How do the Permian ages from our study compare to those from other parts of the Alps?
2. Are two age groups visible also in other regions?
3. What caused the two phases of zircon growth?

The 2DK and Valpelline Series are thought to be closely related to the Ivrea Zone (e.g., Carraro et al. 1970); hence, we start our comparison with the well-documented Permian metamorphism in the Kinzigite Formation of the Ivrea Zone. The Ivrea Zone in the Southern Alps is famous for its cross section through the Permian lower continental curst, displaying a continuous metamorphic field gradient from amphibolite to granulite facies (Kinzigite Formation) as well as mafic underplating (Mafic Complex). Several studies (e.g., Vavra et al. 1999; Peressini et al. 2007; Ewing et al. 2013) show that the main age range of metamorphism is ~316–260 Ma. Ewing et al. (2013) found three

generations of U/Pb zircon ages at 316 ± 3, 276 ± 4, and 258 ± 3 Ma within a granulite facies sample from the Kinzigite Formation. Magmatic ages in the Ivrea Zone show a bimodal age distribution. In the 'central' Ivrea Zone (Val Sesia), the magmatic activity ranges between ~295–280 Ma, with the main intrusive phase at 288 ± 4 Ma (e.g., Peressini et al. 2007; Sinigoi et al. 2011; Klötzli et al. 2014). In the northeastern part of the Ivrea zone (Finero area), magmatic activity was reported at 232 ± 3 Ma (gabbros; Zanetti et al. 2013) and between 212 and 190 Ma (pegmatites; Schaltegger et al. 2015). Our samples from Adria-derived units show a little evidence of the oldest age generation found in the Ivrea Zone (316 ± 3 Ma), though some scattered ages >300 Ma are present in all units that we have studied. Our first, well-defined age group (286–283 Ma) is only present as a partially resolved age peak (~285 Ma) in the Ivrea Zone (Ewing et al. 2013). The intermediate Ivrea age of 276 ± 4 Ma overlaps with our second age group (277–266 Ma) that dominates in the 2DK and Valpelline Series from the present study (Fig. 8). The youngest metamorphic growth generation (258 ± 3 Ma) in the Kinzigite Formation is only slightly younger than our second age peak in the Valpelline Series (266 ± 2 Ma) (Figs. 5, 8). Metamorphic zircon ages younger than 240 Ma in the Ivrea Zone are usually associated with late stage fluid alteration (e.g., Vavra et al. 1996, 1999), similar to what we infer for our scattered ages <260 Ma in the EMC, Valpelline Series, and NE 2DK. We conclude, based on the U/Pb zircon age groups, mineral assemblages, and metamorphic conditions, a similar origin of the Adria-derived units and the Kinzigite Formation of the Ivrea Zone is, indeed, very likely. The cause of the amphibolite to granulite facies metamorphism and the age of metamorphism have long been debated for the Ivrea Zone. Early studies postulated that the metamorphism was caused by the intrusion of the Mafic Complex (e.g., Sinigoi et al. 1991; Henk et al. 1997), but several more recent studies (e.g., Barboza et al. 1999; Barboza and Bergantz 2000; Redler et al. 2012) concluded that these intrusion most likely was not responsible for the regional metamorphism in the Ivrea Zone. The controversy about cause of the age pattern observed in the Ivrea Zone remains as the first phase pre-dates the mafic intrusion by several millions years, and the most abundant age group (~276 Ma) as well as the ~258 Ma ages postdate the intrusion by 10–30 Myr. Similar observations apply in the Malenco unit, a more easterly slice of Adriatic lower continental crust (Fig. 9); Hermann and Rubatto (2003) concluded that the first of three age generations (281 ± 2 Ma) may have been caused by the intrusion of gabbros (281 ± 19 Ma), while subsequent age generations, especially the volumetrically prominent growth generation at 269 ± 3 Ma, required additional heat input, most likely related to lithospheric thinning. The age pattern and observation of age generations clearly postdating the gabbroic intrusions in the Malenco case are similar to what is observed in the Ivrea Zone and, in the present study, in Adria-derived units.

Figure 9 shows a tectonic overview map of the Alps with ages and *P–T* conditions from rocks that experienced Permian HT metamorphism. In addition to the Western Alps, Ivrea Zone, and Malenco unit, notable occurrences in the Austroalpine units of the Eastern Alps are shown, where Permian metamorphism has been recognised with an overall age range of ~290–240 Ma. As in the Ivrea Zone (Vavra et al. 1999; Ewing et al. 2013), the Malenco unit (Hermann and Rubatto 2003), and the Adria-derived units (this study), several growth phases have been established on monazite and detailed Sm/Nd garnet geochronology in the Austroalpine units (e.g., Schuster and Frank 1999; Habler and Thöni 2001; Schuster et al. 2001a, b; Gaidies et al. 2008a, b; Thöni et al. 2008; Thöni and Miller 2009; Schuster et al. 2015). Across the Alpine chain, some units show a broad range of ages (e.g., Valpelline Series, Ivrea Zone, Monte Rosa nappe, Gruf complex, Malenco unit, Rappold complex, Strallegg complex, and Saualpe/Koralpe complex), while other units only show ages from ~290 to 280 Ma (e.g., EMC, Mt. Emilius Klippe, and Campo unit), or only ages <280 Ma (e.g., Matsch unit, Wölz Complex, Plankogel Complex, Jenig Complex, Strieden Complex, and Defereggen Complex). Some Austroalpine units furthest to the east and southeast (Fig. 9) show ages generally younger than 275 Ma, indicating a slight trend towards younger ages from west to east (Fig. 8). As stated above, the absence of a particular age group in a unit does not imply complete absence of it, possibly age groups could get obscured due to few data (unclear significance) or bias during measurements (e.g., analytical resolution, spot size).

In Fig. 9, Permian magmatic ages within the range of ~300–240 Ma are seen to scatter across the Alpine chain. U/Pb zircon ages for felsic and mafic plutons have a median age of 280 Ma and 285 Ma, respectively (Fig. 9; corresponding references in Online Resources 3), while Sm/Nd mineral isochron ages in the Eastern Alps and the Ivrea Zone have a median of ~250 Ma (e.g., Miller and Thöni 1997; Mayer et al. 2000; Miller et al. 2011). U/Pb zircon ages from mafic plutons (visible at the present level of erosion) in the Adria-derived units of the Western Alps are dominantly in the age range of 295–285 Ma. The data presented in this study showed that in the Western Alps, a metamorphic age group (290–280 Ma) is essentially coeval with these magmatic ages (Fig. 8), yet in several units (Valpelline Series, NE, and SW 2DK), a second age group (277–266 Ma) dominates the zircon population (Fig. 8). The fact that abundant and voluminous zircon growth phases as well as detailed Sm/Nd garnet geochronology (Fig. 8) give clearly younger metamorphic ages than the U/Pb zircon intrusion ages does not support to

the often-proposed causal connection, i.e., gabbroic intrusions providing the heat for Permian HT metamorphism in the lower and middle crust of the Adriatic margin.

Several places in the Alps (e.g., Sesia Zone, Ivrea Zone, Malenco unit, or Campo unit; Fig. 9) allow a closer look at the relationship between Permian mafic bodies and Permian metamorphic ages. The EMC in the Sesia Zone hosts several mafic intrusions that were dated to 288 Ma and 285 Ma, the metamorphic ages obtained in this study for the EMC have an average age of 286 ± 2 Ma, this observation support the theory that gabbroic intrusions provided the heat for Permian HT metamorphism. Similar conclusions have been made by Petri (2014) in the Campo unit, where the intrusion of the Sondalo gabbros (289–285 Ma) caused the 288 Ma metamorphism in the surrounding rocks. However, in the Ivrea Zone as well as in the Malenco unit, the mafic intrusions are dated to 288 Ma (Peressini et al. 2007) and 281 Ma (Hansmann et al. 2001), respectively, while metamorphic ages contemporaneous with the intrusion age occur, several phases of voluminous zircon growth up to 20 Myr younger are reported for both units (e.g., Vavra et al. 1999; Hermann and Rubatto 2003; Ewing et al. 2013). Magmatic underplating, pooling of mafic melt at or below the Moho, caused by lithospheric thinning and astenospheric upwelling have been suggested (Henk et al. 1997) to cause regional scale HT metamorphism. This scenario accounts for regional protracted heating, affecting all crustal levels independent of the local occurrence of Permian intrusions. We regard that these intrusions are an effect of magmatic underplating, as well as the HT metamorphism. In areas where magma intruded the shallower (cooler) crustal levels, local contact metamorphism is evident (e.g., in the Campo unit), while at deeper crustal levels (e.g., in the Ivrea Zone), thermal effects around intrusive bodies are less well defined and contact aureoles are hardly distinguishable, due to ambient temperatures being near magmatic temperatures at the time of the intrusion.

The Permian evolution is well represented also in the sedimentary record: early Permian strike-slip tectonics resulted in the opening of asymmetric graben basins in the central part of the South-Alpine unit (e.g., Orobic Basin, Collio Basin; Matte 1986; Massari 1988; Cassinis et al. 1995), with dominantly continental deposits and sparse marine deposits (Bellerophon Formation and Pontebba Supergroup; Bosellini 1991). In summary, the Permian evolution is widely recorded in the Alpine realm, with clear structural, magmatic, metamorphic, and sedimentary signatures, indicating a temporal link between extensional tectonics, the accumulation of mantle melt at the base of the crust (e.g., Malenco unit, Müntener and Hermann 1996; Müntener et al. 2000; Ivrea Zone, Voshage et al. 1990), partial melting in the lower crust (e.g., Ivrea Zone, Redler et al. 2012), intrusion of granitic bodies at higher levels (e.g., Arolla Series, Bussy et al. 1998; Serie dei Laghi, Köppel 1974; Schaltegger and Brack 2007), and explosive acid volcanism at the surface (e.g., Serie dei Laghi, Quick et al. 2009). Although there is a clear temporal link between mafic magmatism and HT metamorphism, the regional scale of the Permian thermal effects—documented over more than 600 km from the Western to the Eastern Alps and further east into the basement of the Pannonian basin (Lelkes-Felvàri et al. 2003)—indicates that the heat source for HT metamorphism was not solely provided by mafic melts intruding the crust, but sustained by the upwelling mantel itself.

## Conclusions and outlook

- This study shows that the Permian thermal evolution is preserved in the Adria-derived units of the Western Alps (EMC, 2DK, Valpelline Series, and Mt. Emilius Klippe), with U/Pb zircon ages ranging from 286 to 266 Ma. Mineral assemblages, trace element thermometry, and zircon growth textures indicate amphibolite to granulite facies conditions (~650–850 °C) and associated partial melting.
- Two different domains could be identified based on their ages. Domain A (EMC, central 2DK, and Mt. Emilius Klippe) shows an age of 286 ± 2 Ma, while domain B (NE and SW 2DK and Valpelline Series) shows a bimodal age distribution of 287–283 and 277–266 Ma.
- The new data set confirms the close similarities between the Valpelline Series, the 2DK, and the Ivrea Zone, as already noted by Carraro et al. (1970) on the basis of metamorphic assemblages. Combined with the previous data, our results indicate contemporaneous HT metamorphism (over 40 Ma) and magmatism in the lower and middle Permian continental crust forming the Adria-derived units of the Alps today. The HT metamorphism and magmatism are the result of the extensional tectonics and high thermal regime that affected the Adriatic plate at Permian time.
- The Variscan evolution in Adria-derived units in the Western Alps still remains to be reassessed. Pervasive Permian or Alpine metamorphic overprint may have obliterated much of the Variscan imprint. Especially, in lower crustal units, prolonged Permian heating most likely erased evidence from the Variscan metamorphic cycle. Zircon geochronology and thermometry might also be useful in elucidating the Variscan remnants in these units.

**Acknowledgements** We thank Thomas Pettke and Afifé El Korh for assistance with LA-ICP-MS work, Martin Robyr for help with EMPA analysis, and Marco Burn and Roland Oberhänsli for providing sample material from the EMC and Mt. Emilius Klippe. Samples VP 74 and VP 66 were collected during Paola Manzotti's M.Sc. thesis supervised by Michele Zucali. Niklaus Grossen, Remo Widmer, Matthias

Bächli, and Rahel Baumann helped with mineral separation; Daniela Rubatto and Bénédicte Cenki-Tok with discussions that helped us improve earlier versions of the manuscript. Ralf Schuster and Geoffroy Mohn are thanked for their constructive reviews. We thank Wolf-Christian Dullo for editorial handling. The Swiss National Science Foundation provided funding (Project 200020-146175).

**Author contributions** Sample material has been collected/provided by B.E. Kunz, P.M., B.vN., M.B., and F.G.; Geochrological and geochemical data have analysed by B.E. Kunz, P.M., and B.vN.; J.R.D. and P.L. provided assistance and discussion with LA-ICP-MS analysis; B.E. Kunz, P.M. and M.E. wrote the paper.

## References

Ayrton S, Bugnon C, Haarpainter T, Weidmann M, Frank E (1982) Géologie du front de la nappe de la Dent-Blanche dans la région des Monts-Dolins, Valais. Eclogae Geol Helv 75:269–286

Babist J, Handy MR, Konrad-Schmolke M, Hammerschmidt K (2006) Precollisional, multistage exhumation of subducted continental crust: The Sesia Zone, western Alps. Tectonics 25:TC6008

Baldwin JA, Brown M, Schmitz MD (2007) First application of titanium-in-zircon thermometry to ultrahigh-temperature metamorphism. Geology 35:295–298

Ballèvre M, Kienast J-R, Vuichard J-P (1986) La « nappe de la Dent-Blanche » (Alpes occidentales): deux unités austroalpines indépendantes. Eclogae Geol Helv 79:57–74

Barboza S, Bergantz G (2000) Metamorphism and Anatexis in the Mafic Complex Contact Aureole, Ivrea Zone, Northern Italy. J Petrol 41:1307–1327

Barboza S, Bergantz G, Brown M (1999) Regional granulite facies metamorphism in the Ivrea zone is the Mafic Complex the smoking gun or a red herring. Geology 27:447–450

Beltrando M, Rubatto D, Compagnoni R, Lister G (2007) Was the Valaisan basin floored by oceanic crust? Evidence of Permian magmatism in the Versoyen Unit (Valaisan domain, NW Alps). Ofioliti 32:85–99

Bertolani MA (1964) Le metamorfiti dell'alta Valle Strona (Provincia di Novara). Period Miner 33:301–336

Bertotti G, Siletto GB, Spalla MI (1993) Deformation and metamorphism associated with crustal rifting: the Permian to Liassic evolution of the Lake Lugano-Lake Como area (Southern Alps). Tectonophysics 226:271–284

Bertrand JM, Paquette J-L, Guillot F (2005) Permian zircon U-Pb ages in the Gran Paradiso massif: revisiting post-Variscan events in the Western Alps. Schw Miner Petrogr Mitt 85:15–29

Bigi G, Carrozzo MT (1990) Structural model of Italy and gravity map. Cons Naz Ric (Italia) 114:3

Bosellini A (1991) Geology of the dolomites: an introduction: Dolomieu conference on carbonate platforms and dolomitization. Tourist Office, Ortisei

Bousquet R, Oberhansli R, Schmid SM, Berger A, Wiederkehr M, Robert C, Rosenberg CL, Koller F, Molli G, Zeilinger G (2012) Metamorphic framework of the Alps. CCGM, Paris

Bussy F, Cadoppi P (1996) U-Pb zircon dating of granitoids from the Dora-Maira massif (western Italian Alps). Schw Miner Petrogr Mitt 76:217–233

Bussy F, Venturini G, Hunziker J, Martinotti G (1998) U-Pb ages of magmatic rocks of the western Austroalpine Dent-Blanche-Sesia unit. Schw Miner Petrogr Mitt 78:163–168

Bussy F, Hernandez J, von Raumer J (2000) Bimodal magmatism as a consequence of the postcollisional readjustment of the thickened Variscan continental lithosphere (Aiguilles Rouges-Mont Blanc Massifs, Western Alps). Trans R Soc Edinb Earth Sci 91:221–233

Carraro F, Dal Piaz GV, Sacchi R (1970) Serie di Valpelline e II Zona Diorito-Kinzigitica sono i relitti di un ricoprimento proveniente dalla zona Ivrea-Verbano. Mem Soc Geol Ital 9:197–224

Cassinis G, Toutin-Morin N, Virgili C (1995) A general outline of the Permian continental basins in Southwestern Europe. In: Scholle P et al (eds) The Permian of Northern Pangea, vol 2. Springer, Berlin, pp 137–157

Cenki-Tok B, Oliot E, Rubatto D, Berger A, Engi M, Janots E, Thomsen TB, Manzotti P, Regis D, Spandler C, Robyr M, Goncalves P (2011) Preservation of Permian allanite within an Alpine eclogite facies shear zone at Mt Mucrone, Italy: mechanical and chemical behavior of allanite during mylonitization. Lithos 125:40–50

Ciarapica G, Passeri L, Bonetto F, Dal Piaz GV (2016) Facies and Late Triassic fossils in the Roisan zone, Austroalpine dent blanche and Mt Mary-Cervino nappe system, NW Alps. Swiss J Geosci 109:1–13

Compagnoni R (1977) The Sesia-Lanzo Zone: high pressure-low temperature metamorphism in the Austroalpine continental margin. Rend Soc Ital Miner Petrol 33:335–374

Compagnoni R, Dal Piaz GV, Hunziker J, Gosso G, Lombardo B, Williams P (1977) The Sesia-Lanzo Zone, a slice of continental crust with Alpine high pressure-low temperature assemblages in the Western Italian Alps. Rend Soc Ital Miner Petrol 33:281–334

Cortiana G, Dal Piaz GV, Del Moro A, Hunziker JC, Martin S (1998) $^{40}$Ar-$^{39}$Ar and Rb-Sr dating of the Pillonet klippe and Sesia-Lanzo basal slice in the Ayas valley and evolution of the Austroalpine-Piedmont nappe stack. Memor Sci Geolog 50:177–194

Dal Piaz GV (1976) Il lembo di recoprimento del Pillonet (falda della Dent Blanche nelle Alpi occidentali). Mem Sci Geol (Padova) 31:1–60

Dal Piaz GV (1999) The Austroalpine-Piedmont nappe stack and the puzzle of Alpine Tethys. Mem Sci Geol 51:155–176

Dal Piaz GV, Nervo R (1971) Il lembo di ricoprimento del Glacier-Rafray (Dent Blanche s.l.). Boll Soc Geol Ital 90:401–414

Dal Piaz GV, Sacchi R (1969) Osservazioni geologiche sul lembo di ricoprimento del Pillonet (Dent Blanche s.l.). Mem Soc Geol Ital 10:257–276

Dal Piaz GV, Gosso G, Martinotti G (1971) La II Zona Dioritokinzigitica tra la Valsesia e la Valle d'Ayas (Alpi occidentali). Memorie della Società Geologica Italiana 11:433–460

Dal Piaz GV, Hunziker J, Martinotti G (1972) La Zona Sesia-Lanzo e l'evoluzione tettonico-metamorfica delle Alpi nordoccidentali interne. Mem Soc Geol Ital 11:433–466

Dal Piaz GV, De Vecchi G, Hunziker J (1977) The austroalpine layered gabbros of the Matterhorn and Mt. Collon-Dents de Bertol. Schw Miner Petrogr Mitt 57:59–88

Dal Piaz GV, Gosso G, Lombardo B (1983) Metamorphic evolution of the Mt. Emilius klippe, Dent Blanche nappe, western Alps. Am J Sci 283A:438–458

Dal Piaz GV, Cortiana G, Del Moro A, Martin S, Pennacchioni G, Tartarotti P (2001) Tertiary age and paleostructural inferences of the eclogitic imprint in the Austroalpine outliers and Zermatt-Saas ophiolite, western Alps. Int J Earth Sci 90:668–684

Dal Piaz GV, Gianotti F, Monopoli B, Pennacchioni G, Tartarotti P, Schiavo A (2010) Note illustrative della Carta Geologica d'Italia alla scala 1: 50.000, Foglio 091 Chatillon. Servizio Geologico d'Italia Foglio 91:5–152

De Leo S, Biino G, Compagnoni R (1987) Riequilibrazioni metamorfiche alpine nella serie di Valpelline e di Arolla a Nord di Bionaz (Valpelline-Aosta). Rend Soc Ital Miner Petrol 42:181–182

Desmons J, Compagnoni R, Cortesogno L, Frey M, Gaggero L (1999) Pre-Alpine metamorphism of the Internal zones of the Western Alps. Schw Miner Petrogr Mitt 79:23–39

Diehl E, Masson R, Stutz A (1952) Contributo alla conoscenza del ricoprimento della Dent Blanche. Memorie degli Istituti di Geologia e Mineralogia dell'Universita di Padova 17:1–52

Diella V, Spalla MI, Tunesi A (1992) Contrasting thermomechanical evolutions in the Southalpine metamorphic basement of the Orobic Alps (Central Alps, Italy). J Metamorph Geol 10:203–219

Engi M, Scherrer N, Burri T (2001) Metamorphic evolution of pelitic rocks of the Monte Rosa nappe: constraints from petrology and single grain monazite age data. Schw Miner Petrogr Mitt 81:305–328

Ewing TA, Hermann J, Rubatto D (2013) The robustness of the Zr-in-rutile and Ti-in-zircon thermometers during high-temperature metamorphism (Ivrea-Verbano Zone, northern Italy). Contrib Miner Petrol 165:757–779

Ewing TA, Rubatto D, Beltrando M, Hermann J (2015) Constraints on the thermal evolution of the Adriatic margin during Jurassic continental break-up: U-Pb dating of rutile from the Ivrea-Verbano Zone, Italy. Contrib Miner Petrol 169:1–22

Fountain D (1976) The Ivrea-Verbano and Strona-Ceneri Zones, Northern Italy: a cross-section of the continental crust-New evidence from seismic velocities of rock samples. Tectonophysics 33:145–165

Frisch W, Neubauer F (1989) Pre-Alpine terranes and tectonic zoning in the eastern Alps. Geol Soc Am Spec Pap 230:91–100

Gaidies F, Krenn E, De Capitani C, Abart R (2008a) Coupling forward modelling of garnet growth with monazite geochronology: an application to the Rappold Complex (Austroalpine crystalline basement). J Metamorph Geol 26:775–793

Gaidies F, De Capitani C, Abart R, Schuster R (2008b) Prograde garnet growth along complex P-T–t paths: results from numerical experiments on polyphase garnet from the Wölz Complex (Austroalpine basement). Contrib Miner Petrol 155:673–688

Galli A, Le Bayon B, Schmidt M, Burg J-P, Caddick M, Reusser E (2011) Granulites and charnockites of the Gruf Complex: evidence for Permian ultra-high temperature metamorphism in the Central Alps. Lithos 124:17–45

Galli A, Le Bayon B, Schmidt M, Burg J-P, Reusser E, Sergeev S, Larionov A (2012) U-Pb zircon dating of the Gruf Complex: disclosing the late Variscan granulitic lower crust of Europe stranded in the Central Alps. Contrib Miner Petrol 163:353–378

Gardien V, Reusser E, Marquer D (1994) Pre-alpine Metamorphic Evolution of the Gneisses From the Valpelline Series (western Alps, Italy). Schw Miner Petrogr Mitt 74:489–502

Giuntoli F (2016) Assembly of continental fragments during subduction at HP: Metamorphic history of the cetral Sesia Zone (NW Alps). PhD thesis, University of Bern, Switzerland

Giuntoli F, Engi M (2016) Internal geometry of the central Sesia Zone (Aosta Valley, Italy): HP tectonic assembly of continental slices. Swiss J Geosci 109:445–471

Gosso G (1977) Metamorphic evolution and fold history in the eclogitic micaschists of the upper Gressoney valley (Sesia-Lanzo zone, Western Alps). Rendiconti della Societa Italiana di Mineralogia e Petrologia 33:389–407

Gosso G, Messiga B, Rebay G, Spalla M (2010) Interplay between deformation and metamorphism during eclogitization of amphibolites in the Sesia-Lanzo Zone of the Western Alps. Int Geol Rev 52:1193–1219

Grossen N (2012) Polymetamorphic evolution of the Australpine Pillonet Klippe in the Western Alps (Val d'Ayas, Northern Italy). MSc thesis, University of Bern, Switzerland

Habler G, Thöni M (2001) Preservation of Permo-Triassic low-pressure assemblages in the Cretaceous high-pressure metamorphic Saualpe crystalline basement (Eastern Alps, Austria). J Metamorph Geol 19:679–697

Habler G, Thöni M, Grasemann B (2009) Cretaceous metamorphism in the Austroalpine Matsch Unit (Eastern Alps): the interrelation between deformation and chemical equilibration processes. Mineral Petrol 97:149–171

Handy MR, Schmid SM, Bousquet R, Kissling E, Bernoulli D (2010) Reconciling plate-tectonic reconstructions of Alpine Tethys with the geological-geophysical record of spreading and subduction in the Alps. Earth Sci Rev 102:121–158

Hansmann W, Müntener O, Hermann J (2001) U-Pb zircon geochronology of a tholeiitic intrusion and associated migmatites at a continental crust-mantle transition, Val Malenco, Italy. Schw Miner Petrogr Mitt 81:239–255

Harley S (2008) Refining the P-T records of UHT crustal metamorphism. J Metamorph Geol 26:125–154

Harley SL, Kelly NM, Möller A (2007) Zircon behaviour and the thermal histories of mountain chains. Elements 3:25–30

Heede H-U (1997) Isotopengeologische Untersuchungen an Gesteinen des ostalpinen Saualpenkristallins, Kärnten. Österreich Münster Forsch Geol Paläont 81:1–168

Henk A, Franz L, Teufel S, Oncken O (1997) Magmatic underplating, extension, and crustal reequilibration: insights from a cross-section through the Ivrea Zone and Strona-Ceneri Zone, Northern Italy. J Geol 105:367–377

Hermann J, Rubatto D (2003) Relating zircon and monazite domains to garnet growth zones: age and duration of granulite facies metamorphism in the Val Malenco lower crust. J Metamorph Geol 21:833–852

Hunziker J (1974) Rb-Sr and K-Ar age determination and the alpine tectonic history of the western alps. Memorie degli Istituti di Geologia e Mineralogia dell'Universita di Padova 31:1–45

Kiénast JR, Nicot E (1971) Présence d'une paragenese adisthene et chloritoıde (d'âge alpin probable) dans les gneiss asillimanite, grenat et cordiérite de Valpelline (Val d'Aoste, Italie). C R Acad Sci Paris D 272:1836–1840

Klötzli US, Sinigoi S, Quick JE, Demarchi G, Tassinari CC, Sato K, Günes Z (2014) Duration of igneous activity in the Sesia Magmatic System and implications for high-temperature metamorphism in the Ivrea-Verbano deep crust. Lithos 206–207:19–33

Köppel V (1974) Isotopic U-Pb ages of monazites and zircons from the crust-mantle transition and adjacent units of the ivrea and ceneri zones (Southern Alps, Italy). Contrib Miner Petrol 43:55–70

Kretz R (1983) Symbols for rock-forming minerals. Am Miner 68:277–279

Kunz BE, Johnson TE, White RW, Redler C (2014) Partial melting of metabasic rocks in Val Strona di Omegna, Ivrea Zone, northern Italy. Lithos 190–191:1–12

Lardeaux JM (1981) Evolution Tectono-métamorphique de la zone nord du massif de Sésia-Lanzo (Alpes Occidentales): un exemple d'eclogitisation de croute continentale. Ph.D. dissertation, Université de Paris, Mémoires des Sciences de la Terre, Paris

Lardeaux JM, Spalla MI (1991) From granulites to eclogites in the Sesia zone (Italian Western Alps): a record of the opening and closure of the Piedmont ocean. J Metamorph Geol 9:35–59

Lardeaux JM, Gosso G, Kienast JR, Lombardo B (1982) Relations entre le metamorphisme et la deformation dans la zone Sesia-Lanzo (Alpes Occidentales) et le probleme de l'eclogitisation

de la croute continentale. Bulletin de la Société géologique de France 4:793–800

Lelkes-Felvàri G, Frank W, Schuster R (2003) Geochronological constraints of the Variscan, Permian-Triassic and eo-Alpine (Cretaceous) evolution of the great Hungarian Plain Basment. Geologica Carpathia 54:299–315

Ludwig KR (2003) Isoplot/Ex version 3.0. A geochronological toolkit for Microsoft Excel Geochronological Centre Special Publication. Geochronological Centre, Berkeley, p 70

Luvizotto GL, Zack T (2009) Nb and Zr behavior in rutile during high-grade metamorphism and retrogression: an example from the Ivrea-Verbano Zone. Chem Geol 261:303–317

Mair V, Schuster R, Tropper P (2003) The metamorphic evolution of the Ortler crystalline. Mitteilungen der Österreichischen Mineralogischen Gesellschaft 148:215–217

Manzotti P (2011) Petro-structural map of the Dent Blanche tectonic system between Valpelline and Valtournenche valleys, Western Italian Alps. J Maps 7:340–352

Manzotti P (2012) Polycyclic Evolution in the Dent Blanche Tectonic System. PhD thesis, University of Bern, Switzerland

Manzotti P, Zucali M (2013) The pre-Alpine tectonic history of the Austroalpine continental basement in the Valpelline unit (Western Italian Alps). Geol Mag 150:153–172

Manzotti P, Rubatto D, Darling J, Zucali M, Cenki-Tok B, Engi M (2012) From Permo-Triassic lithospheric thinning to Jurassic rifting at the Adriatic margin: petrological and geochronological record in Valtournenche (Western Italian Alps). Lithos 146–147:276–292

Manzotti P, Ballèvre MZ, Robyr M, Engi M (2014a) The tectonometamorphic evolution of the Sesia-Dent Blanche nappes (internal Western Alps): review and synthesis. Swiss J Geosci 107:309–336

Manzotti P, Zucali M, Ballevre M, Robyr M, Engi M (2014b) Geometry and kinematics of the Roisan-Cignana Shear Zone, and the orogenic evolution of the Dent Blanche Tectonic System (Western Alps). Swiss J Geosci 107:1–25

Marotta AM, Spalla MI (2007) Permian-Triassic high thermal regime in the Alps: result of late Variscan collapse or continental rifting? Validation by numerical modeling. Tectonics 26:TC4016

Massari F (1988) Some thoughts on the Permo-Triassic evolution of the South-Alpine area. Memorie della Società Geologica Italiana 34:179–188

Matte P (1986) Tectonics and plate tectonics model for the Variscan belt of Europe. Tectonophysics 126:329–374

Mayer A, Mezger K, Sinigoi S (2000) New Sm-Nd ages for the Ivrea-Verbano Zone, Sesia and Sessera valleys (Northern-Italy). J Geodyn 30:147–166

Mehnert KR (1975) The Ivrea Zone: a model of the deep crust. Neues Jahrbuch Mineralogische Abhandlungen 125:156–199

Miller C, Thöni M (1997) Eo-Alpine eclogitisation of Permian MORB-type gabbros in the Koralpe (Eastern Alps, Austria): new geochronological, geochemical and petrological data. Chem Geol 137:283–310

Miller C, Thöni M, Goessler W, Tessadri R (2011) Origin and age of the Eisenkappel gabbro to granite suite (Carinthia, SE Austrian Alps). Lithos 125:434–448

Monjoie P, Bussy F, Schaltegger U, Mulch A, Lapierre H, Pfeifer HR (2007) Contrasting magma types and timing of intrusion in the Permian layered mafic complex of Mont Collon (Western Alps, Valais, Switzerland): evidence from U/Pb zircon and $^{40}Ar/^{39}Ar$ amphibole dating. Swiss J Geosci 100:125–135

Müntener O, Hermann J (1996) The Val Malenco lower crust-upper mantle complex and its field relations (Italian Alps). Schw Miner Petrogr Mitt 76:475–500

Müntener O, Hermann J (2001) The role of lower crust and continental upper mantle during formation of non-volcanic passive margins: evidence from the Alps. Geol Soc 187:267–288

Müntener O, Hermann J, Trommsdorff V (2000) Cooling history and exhumation of lower-crustal granulite and upper mantle (Malenco, Eastern Central Alps). J Petrol 41:175–200

Neubauer F, Frisch W, Schmerold R, Schloeser H (1989) Metamorphosed and dismembered ophiolite suites in the basement units of the Eastern Alps. Tectonophysics 164:49–62

Nicot E (1977) Les roches meso et catazonales de la Valpelline (nappe de la Dent Blanche, Alpes italiennes). PhD thesis, Université de Paris VI, France

Paquette J-L, Chopin C, Peucat J-J (1989) U-Pb zircon, Rb-Sr and Sm-Nd geochronology of high-to very-high-pressure meta-acidic rocks from the Western Alps. Contrib Miner Petrol 101:280–289

Peressini G, Quick JE, Sinigoi S, Hofmann AW, Fanning M (2007) Duration of a large mafic intrusion and heat transfer in the lower crust: a SHRIMP U-Pb Zircon Study in the Ivrea-Verbano Zone (Western Alps, Italy). J Petrol 48:1185–1218

Pesenti C, Zucali M, Manzotti P, Diella V, Risplendente A (2012) Linking U-Th-Pb monazite dating to partial melting microstructures: application to the Valpelline Series (Austroalpine domain, Western Alps). Rendiconti Online Societa Geologica Italiana 22:183–185

Petri B (2014) Formation et exhumation des granulites permiennes: établir les conditions pré-rift et déterminer l'histoire d'exhumation syn-rift. PhD thesis, University of Strasbourg, France

Pfiffner A (2009) Geologie der Alpen. Haupt Verlag, Bern

Pognante U, Talarico F, Benna P (1988) Incomplete blueschist recrytallization in high-grade metamorphics from the Sesia-Lanzo unit (Vasario-Sparone subunit, Western Alps): a case history of metastability. Lithos 21:129–142

Quick JE, Sinigoi S, Mayer A (1995) Emplacement of mantle peridotite in the lower continental crust, Ivrea-Verbano zone, northwest Italy. Geology 23:739–742

Quick JE, Sinigoi S, Snoke AW, Kalakay TJ, Mayer A, Peressini G (2003) Geologic map of the southern Ivrea-Verbano Zone, Northwestern Italy. USGS I-2776:1-22. USGS, Washington, DC

Quick JE, Sinigoi S, Peressini G, Demarchi G, Wooden JL, Sbisà A (2009) Magmatic plumbing of a large Permian caldera exposed to a depth of 25 km. Geology 37:603–606

Reddy SM, Kelley SP, Wheeler J (1996) A $^{40}Ar/^{39}Ar$ laser probe study of micas from the Sesia Zone, Italian Alps: implications for metamorphic and deformation histories. J Metamorph Geol 14:493–508

Redler C, Johnson TE, White RW, Kunz BE (2012) Phase equilibrium constraints on a deep crustal metamorphic field gradient: metapelitic rocks from the Ivrea Zone (NW Italy). J Metamorph Geol 30:235–254

Regis D, Rubatto D, Darling J, Cenki-Tok B, Zucali M, Engi M (2014) Multiple metamorphic stages within an eclogite-facies Terrane (Sesia Zone, Western Alps) revealed by Th-U-Pb petrochronology. J Petrol 55:1429–1456

Ridley J (1989) Structural and metamorphic history of a segment of the Sesia-Lanzo zone, and its bearing on the kinematics of Alpine deformation in the western Alps. Geol Soc 45:189–201

Rivalenti G, Rossi A, Siena F, Sinigoi S (1984) The layered series of the Ivrea-Verbano igneous complex, western Alps, Italy. Tschermaks Mineralogische und Petrographische Mitteilungen 33:77–99

Roberts MP, Finger F (1997) Do U-Pb zircon ages from granulites reflect peak metamorphic conditions? Geology 25:319–322

Robyr M, Darbellay B, Baumgartner LP (2014) Matrix-dependent garnet growth in polymetamorphic rocks of the Sesia zone, Italian Alps. J Metamorph Geol 32:3–24

Rockenschaub M, Kolenprat B, Frank W (1999) The tectonometamorphic evolution of Austroalpine units in the Brenner area (Tirol, Austria) new geochronological implications. Tübinger geowissenschaftliche Arbeiten Serie A 52:118–119

Rubatto D (2002) Zircon trace element geochemistry: partitioning with garnet and the link between U-Pb ages and metamorphism. Chem Geol 184:123–138

Rubatto D, Gebauer D, Fanning M (1998) Jurassic formation and Eocene subduction of the Zermatt-Saas-Fee ophiolites: implications for the geodynamic evolution of the Central and Western Alps. Contrib Miner Petrol 132:269–287

Rubatto D, Gebauer D, Compagnoni R (1999) Dating of eclogite-facies zircons: the age of Alpine metamorphism in the Sesia-Lanzo Zone (Western Alps). Earth Planet Sci Lett 167:141–158

Rubatto D, Williams IS, Buick IS (2001) Zircon and monazite response to prograde metamorphism in the Reynolds Range, central Australia. Contrib Miner Petrol 140:458–468

Sawyer EW (2008) Atlas of migmatites. The Canadian Mineralogist, Special Publications 9. NRC Research Press, Ottawa

Schaltegger U, Brack P (2007) Crustal-scale magmatic systems during intracontinental strike-slip tectonics: U, Pb and Hf isotopic constraints from Permian magmatic rocks of the Southern Alps. Contrib Miner Petrol 96:1131–1151

Schaltegger U, Ulianov A, Müntener O, Ovtcharova M, Peytcheva I, Vonlanthen P, Vennemann T, Antognini M, Girlanda F (2015) Megacrystic zircon with planar fractures in miaskite-type nepheline pegmatites formed at high pressures in the lower crust (Ivrea Zone, southern Alps, Switzerland). Am Miner 100:83–94

Schmerold R (1988) Die Plankogel-Serie im ostalpinen Kristallin in Kor- und Saualpe (Kärnten-Steiermark-Österreich) als ophiolitische Sutur. PhD thesis, University of Tübigen, Germany

Schmid R, Wood BJ (1976) Phase relationships in granulitic metapelites from the Ivrea-Verbano zone (Northern Italy). Contrib Miner Petrol 54:255–279

Schmid SM, Fügenschuh B, Kissling E, Schuster R (2004) Tectonic map and overall architecture of the Alpine orogen. Eclogae Geol Helv 97:93–117

Schuster R, Frank W (1999) Metamorphic evolution of the Austroalpine units east of the Tauern Window: indications for Jurassic strike slip tectonics. Mitteilungen der Gesellschaft der Geologie- und Bergbaustudenten in Österreich 42:37–58

Schuster R, Stüwe K (2008) Permian metamorphic event in the Alps. Geology 36:603–606

Schuster R, Scharbert S, Abart R, Frank W (2001a) Permo-Triassic extension and related HT/LP metamorphism in the Austroalpine-Southalpine realm. Mitteilungen der Geologie und Bergbaustudenten Österreichs 45:111–141

Schuster R, Proyer A, Hoinkes G, Schulz B (2001b) Indications for a Permo-Triassic metamorphic imprint in the Austroalpine crystalline rocks of the Defferegggen Alps (Eastern Tyrol). Mitteilungen der Österreichischen Mineralogischen Gesellschaft 146

Schuster R, Tropper P, Krenn E, Finger F, Frank W, Philippitsch R (2015) Prograde Permo-Triassic metamorphic HT/LP assemblages from the Austroalpine Jenig Complex (Carinthia, Austria). Aust J Earth Sci 108:73–90

Siegesmund S, Layer P, Dunkl I, Vollbrecht A, Steenken A, Wemmer K, Ahrendt H (2008) Exhumation and deformation history of the lower crustal section of the Valstrona di Omegna in the Ivrea Zone, southern Alps. Geol Soc 298:45–68

Sills J (1984) Granulite Facies Metamorphism in the Ivrea Zone, N.W. Italy. Schw Miner Petrogr Mitt 64:169–191

Sinigoi S, Antonini P, Demarchi G, Longinelli A, Mazzucchelli M, Negrini L, Rivalenti G (1991) Intractions of mantle and crustal magmas in the southern part of the Ivrea Zone (Italy). Contrib Miner Petrol 108:385–395

Sinigoi S, Quick JE, Clemens-Knott D, Mayer A, Demarchi G, Mazzucchelli M, Nehrini L, Rivalenti G (1994) Chemical evolution of a large mafic intrusion in the lower crust, Ivrea-Verbano Zone, northern Italy. J Geophys Res 99:21575–21590

Sinigoi S, Quick JE, Demarchi G, Klötzli U (2011) The role of crustal fertility in the generation of large silicic magmatic systems triggered by intrusion of mantle magma in the deep crust. Contrib Miner Petrol 162:691–707

Spalla MI, Lardeaux J-M, Dal Piaz GV, Gosso G (1991) Metamorphisme et tectonique a la marge externe de la zone Sesia-Lanzo (Alpes occidentales). Mem Sci Geol 43:361–369

Spalla MI, Zanoni D, Marotta A, Rebay G, Roda M, Zucali M, Gosso G (2014) The transition from Variscan collision to continental break-up in the Alps: insights from the comparison between natural data and numerical model predictions. Geol Soc 405:363–400

Stünitz H (1989) Partitioning of metamorphism and deformation in the boundary region of the "Seconda Zona Diorito-Kinzigitica", Sesia Zone, Western Alps. PhD thesis, ETH Zürich, Switzerland

Thöni M (1999) A review of geochronological data from the Eastern Alps. Schw Miner Petrogr Mitt 79:209–230

Thöni M, Miller C (2009) The "Permian event" in the Eastern European Alps: Sm-Nd and P-T data recorded by multi-stage garnet from the Plankogel unit. Chem Geol 260:20–36

Thöni M, Miller C, Zanetti A, Habler G, Goessler W (2008) Sm-Nd isotope systematics of high-REE accessory minerals and major phases: ID-TIMS, LA-ICP-MS and EPMA data constrain multiple Permian-Triassic pegmatite emplacement in the Koralpe, Eastern Alps. Chem Geol 254:216–237

Vavra G, Schaltegger U (1999) Post-granulite facies monazite growth and rejuvenation during Permian to Lower Jurassic thermal and fluid events in the Ivrea Zone (Southern Alps). Contrib Miner Petrol 134:405–414

Vavra G, Gebauer D, Schmid R, Compston W (1996) Multiple zircon growth and recrystallization during polyphase Late Carboniferous to Triassic metamorphism in granulites of the Ivrea Zone (Southern Alps): an ion microprobe (SHRIMP) study. Contrib Miner Petrol 122:337–358

Vavra G, Schmid R, Gebauer D (1999) Internal morphology, habit and U-Th-Pb microanalysis of amphibolite-to-granulite facies zircons: geochronology of the Ivrea Zone (Southern Alps). Contrib Miner Petrol 134:380–404

von Raumer JF, Bussy F, Schaltegger U, Schulz B, Stampfli GM (2013) Pre-Mesozoic Alpine basements—their place in the European Paleozoic framework. Geol Soc Am Bull 125:89–108

Voshage H, Hofmann AW, Mazzucchelli M, Rivalenti G, Sinigoi S, Raczek I, Demarchi G (1990) Isotopic evidence from the Ivrea Zone for a hybrid lower crust formed by magmatic underplating. Nature 347:731–736

Vuichard JP (1987) Conditions P-T du métamorphisme anté-alpin dans la « seconde zone dioritokinzigitique » (Zone Sesia-Lanzo, Alpes occidentales). Schw Miner Petrogr Mitt 67:257–271

Vuichard J-P (1989) La marge austroalpine durant la collision alpine: évolution tectonométamorphique de la zone de Sesia-Lanzo. Mémoires et Documents du Centre Armoricain d'Etude Structurale des Socles (Rennes) 24:307

Watson EB, Wark DA, Thomas JB (2006) Crystallization thermometers for zircon and rutile. Contrib Miner Petrol 151:413–433

Williams P, Compagnoni R (1983) Deformation and metamorphism in the Bard area of the Sesia Lanzo Zone, Western Alps, during subduction and uplift. J Metamorph Geol 1:117–140

Yakymchuk C, Brown M (2014) Behaviour of zircon and monazite during crustal melting. J Geol Soc Lond 171:465–479

Zanetti A, Mazzucchelli M, Sinigoi S, Giovanardi T, Peressini G, Fanning M (2013) SHRIMP U-Pb Zircon Triassic Intrusion Age of the Finero Mafic Complex (Ivrea-Verbano Zone, Western Alps) and its Geodynamic Implications. J Petrol 54:2235–2265

Zingg A (1980) Regional Metamorphism in the Ivrea Zone (Southern Alps, N-Italy): field and microscopic Investigations. Schw Miner Petrogr Mitt 60:153–179

Zucali M (2011) Coronitic microstructures in patchy eclogitised continental crust: the Lago della Vecchia pre-Alpine metagranite (Sesia-Lanzo Zone, Western Italian Alps). J Virtual Explor 38:3–28

Zucali M, Spalla MI, Gosso G (2002) Strain partitioning and fabric evolution as a correlation tool: the example of the Eclogitic Micaschists Complex in the Sesia-Lanzo Zone (Monte Mucrone-Monte Mars, Western Alps, Italy). Schw Miner Petrogr Mitt 82:429–454

Zucali M, Manzotti P, Diella V, Pesenti C, Risplendente A, Darling J, Engi M (2011) Permian tectonometamorphic evolution of the Dent Blanche Unit (Austroalpine domain, Western Italian Alps). Rendiconti Online Societa Geologica Italiana 15:133–136